CFA/HEA 78-214

THE HEAO-B X-RAY OBSERVATORY
SUMMARY OF INSTRUMENT PERFORMANCE AND GUEST OBSERVER'S GUIDE

Prepared by the HEAO-B Consortium Institutions:

Harvard-Smithsonian Center for Astrophysics

Center for Space Research - Massachusetts Institute of Technology

Columbia Astrophysical Laboratory - Columbia University

Laboratory for High Energy Astrophysics - Goddard Space Flight Center

Riccardo Giacconi
Principal Investigator

Ethan J. Schreier
Senior Project Scientist/Mission Operations

Frederick D. Seward
Guest Observer Program Coordinator

This is a revision of

CFA/HEA 76-143

The information in the previous edition is no longer valid.
It should be replaced in its entirity by this document.

TABLE OF CONTENTS

I. INTRODUCTION

The launch in 1978 of the HEAO-B X-ray Observatory will provide astronomers with a substantial facility capable of carrying out detailed studies with a sensitivity some 10^3 times greater than that currently achieved.

The Observatory incorporates a high resolution X-ray telescope and a focal plane assembly capable of positioning at the focus one of four instruments: a high resolution imaging detector (HRI), a broader field imaging proportional counter (IPC), a solid state spectrometer (SSS), and a Bragg crystal spectrometer (FPCS). It also includes a monitor proportional counter (MPC) aligned with the telescope, broadband filter (BBFS) and objective grating (OGS) spectrometers to be used with the imaging detectors, and an active attitude system capable of arc minute pointing and arc second attitude determination.

The Observatory is under the scientific direction of the HEAO-B Consortium Institutions: Harvard-Smithsonian Center for Astrophysics, Center for Space Research/ Massachusetts Institute of Technology, Columbia Astrophysical Laboratory/Columbia University, and Laboratory for High Energy Astrophysics/Goddard Space Flight Center. The Principal Scientists are E. Boldt (GSFC), G. Clark (MIT), R. Giacconi (SAO), H. Gursky (SAO), and R. Novick (CAL). The Principal Investigator, R. Giacconi of the Smithsonian Astrophysical Observatory, will act as the Director of the Observatory. The project is under the management of NASA's Marshall Space Flight Center, with major hardware support from American Science & Engineering and from TRW.

The utilization of this facility by a broad segment of the astronomical scientific community is an essential element in obtaining a full scientific return commensurate with its capabilities. For this reason a Guest Observer Program has been started and 20% of the total effective observing time will be made available to this program during the first year of the mission. 20% of the first year's observing time is about 3×10^6s. If the average observational time for a given program is $\sim 10^4$s, 300 different observing programs can be carried out by Guest Observers during the first year. It is anticipated that 50% of the time will be available to Guest Observers should the mission continue past the first year.

In addition to these independent observations, the entire data set will be open for collaborative study. We are making available the planned Consortium Observing Program (Appendix D); prospective Guest Observers may thus determine whether independent observations or collaborations are appropriate.

We recognize that the size of the Consortium program may at first glance produce a discouraging effect on potential Guest Observers. The instruments are quite sensitive and it does not take much time to examine a particular object. The program was set up to cover basic measurements of interest to most X-ray astronomers and thus samples a wide variety of astronomical phenomena. It is extremely broad in its objectives, but only thorough in a few selected areas of research, such as the deep survey. This will explore for the first time a new sensitivity range, and likely find many new faint sources important to extragalactic studies and cosmology.

The fact that observations of a particular object or class of objects appears in our observational program, should not at all be considered a deterrent for either cooperative, independent, or complementary research efforts by potential Guest

Observers. It has been our experience when discussing the observational program with colleagues that extensions and deepening of the research program immediately come to mind in a natural manner. We are hopeful that creative and fruitful collaborations can be established with a large number of astronomers on this basis.

Given the nature of the program and the need to coordinate the activity of individuals at several NASA centers and research institutions, a certain bureaucratic procedure appears inevitable. We will make every effort on our part to simplify this process and make this program as close to a scientist-to-scientist collaborative effort as feasible.

II. POLICIES AND PROCEDURES

These are given in the NASA Space Science Notice dated June 7, 1978. In brief:

Proposals for Guest Observer status should be submitted to NASA Headquarters for review and approval. A technical Observing Proposal should be included, specifying the target or targets to be observed, the appropriate instrument configuration, the total required observing time and/or observing window, a short discussion of the feasibility of the observation, and a scientific justification of the request.

Prospective Guest Observers may find it convenient (but are not required) to send a copy of the technical Observing Proposal directly to the HEAO-B Mission Operations Office at the Harvard-Smithsonian Center for Astrophysics; this will facilitate the evaluation of technical feasibility and scheduling of observing time. The desired format for observing proposals, and a list of scientific categories, is included in Appendix A.

Proposals are expected to fall into three categories of participation:

A) Correlative Studies - Astrophysical data obtained independently by a Guest Observer from objects or phenomena also observed by HEAO-B would be used in collaboration with data from one or more HEAO investigators to provide a more complete data base from which interpretations could be derived. These data may be from radio, infrared or optical ground-based observations, from rocket or balloon observations, or from pre-existing data.

B) Research Using Consortium Data - A Guest Observer would utilize data from existing Consortium observations, probably in direct collaboration with a Consortium Scientist. For example, deep surveys containing several hundred sources may be of interest to several investigators from different points of view. There are also probably many areas in which scientific objectives of Guest Observers are the same as those of Consortium members who have acquired the data, and cooperative investigations may be mutually beneficial.

C) Guest Observations - A Guest Observer would propose observations of a specific object or region with one or more HEAO-B instruments. The resulting data would be made available to him. Immediately after initial check-out and in-flight calibration of the observatory, approximately 20 percent of the total observing time will be made available to Guest Observers in this category.

It is expected that no extensive surveys will be proposed by a Guest Observer. Not only are such surveys already planned by the Consortium, but they would unfairly limit the time available for other Observers.

NASA will form a Review Committee to evaluate the proposals for HEAO-B Guest Observations. This committee, with technical input from the Consortium,

will judge proposals for scientific merit, feasibility of the intended research, and conflict with observations planned by both the Consortium and other Guest Observers. Conflicts will be resolved as follows:

1) If an observation of a requested target is already planned by a Consortium member, or by another Guest Observer, then:

a) For the same scientific objective, the desirability of a scientific collaboration will be left to the appropriate Consortium members, or to the two Guest Observers (earlier request having priority).

b) For different scientific objectives, the data relevant to these objectives will be made available to the Guest Observer.

2) If the observing time window required is allocated to a different observation planned by a Consortium member (within Consortium allocation), if neither observation can be rescheduled, and if both are of equal scientific merit, the proposal will be rejected. The rationale for the decision will be transmitted to the Guest Observer along with suggestions for modifications of the observing program to resolve the conflict.

3) If the observing time window has also been requested by another Guest Observer for a different target, then the proposals will be judged on scientific merit.

Guest Observer proposals will be sent to the HEAO Project Office at the Marshall Space Flight Center, and to the HEAO-B Mission Operations Office at the Harvard-Smithsonian Center for Astrophysics for review of technical feasibility and for determination of conflicts with already planned observations.

To the maximum extent possible, all reasonable proposals will be accepted, subject to observing time and funding constraints. It is hoped that most conflicts can be settled by the parties involved. If this is impossible, external referees will be used according to established scientific practice.

Approved proposals will be integrated into the overall observing plan for the Observatory which will be prepared by the HEAO-B Mission Operations office at the SAO.

The first six months of observations will be planned 3 months before launch, the second six months, 3 months after launch, etc. A detailed plan for any given time will be ready several weeks in advance of the actual observations. Guest observations are most easily incorporated at the start of this process, 3 to 9 months before the observation. It will be difficult to include new observations at a later time so early communication of proposed observations is encouraged.

Data obtained from the Observatory for the Guest Observer Program will be received by the HEAO-B Data Processing Facility at SAO. Limited computer time, programming assistance, and scientific liaison will be available at SAO for Guest Observers.

Some funds will be available from NASA for travel to and from SAO or for data analysis at the Guest Observers' home institution. The NASA Space Science Notice dated June 7, 1978 gives details for submitting proposals. Applications for support should be directed to NASA Headquarters, simultaneously with the submission of the technical observing proposal.

During Observatory operations, a Users Committee will be established, consisting of Consortium members and representatives of the Guest Observers to help resolve any problems incurred in the course of the program. Final responsibility

for the resolution of conflicts, as well as for other aspects of Observatory operations, rests with NASA and the Director of the Observatory.

Requests for further technical information should be directed to:

Dr. Frederick D. Seward

Harvard-Smithsonian Center for Astrophysics

60 Garden Street

Cambridge, Massachusetts 02138

Telephone: (617) 495-7282, FTS 830-7282

III. EXPERIMENT DESCRIPTION AND SENSITIVITIES

The HEAO-B X-ray telescope consists of a high resolution mirror assembly, a focal plane transport assembly capable of positioning one of four X-ray instruments at the telescope focus, a monitor proportional counter aligned with the telescope, broad band filter and objective grating spectrometers which can be used in conjunction with focal plane instruments and an aspect system. Each of the focal plane instruments operating along with auxiliary systems stress one or more of the measurement capabilities of the Observatory: precise location, angular size and structure, energy spectra, and time variability. Figure 1 shows the configuration of the HEAO-B Observatory, and Table 1 summarizes the capabilities of the Observatory.

The approximate sensitivity of the imaging instruments for detection of sources is summarized in Figure 2. The smallest indicated source sizes, 3' x 3' (IPC) and 12" x 12" (HRI) are the optimum cell sizes for the detection of faint point sources.

The source strength is given in UHURU counts. Since the HEAO-B imaging detectors are sensitive to soft X-rays (0.2 to 2 keV) and UHURU was not, the relative sensitivity depends strongly on the low energy cut-off parameter, Ea. To generate Figure 2 the conversion factors used were:

$$1 \text{ IPC ct/sec} = 1 \text{ UHURU ct/sec}$$

$$1 \text{ HRI ct/sec} = 10 \text{ UHURU ct/sec}$$

These correspond to a $E_a = 0.3$ or $N_H = 5 \times 10^{20}$.

505-082

HEAO-B EXPERIMENT CONFIGURATION

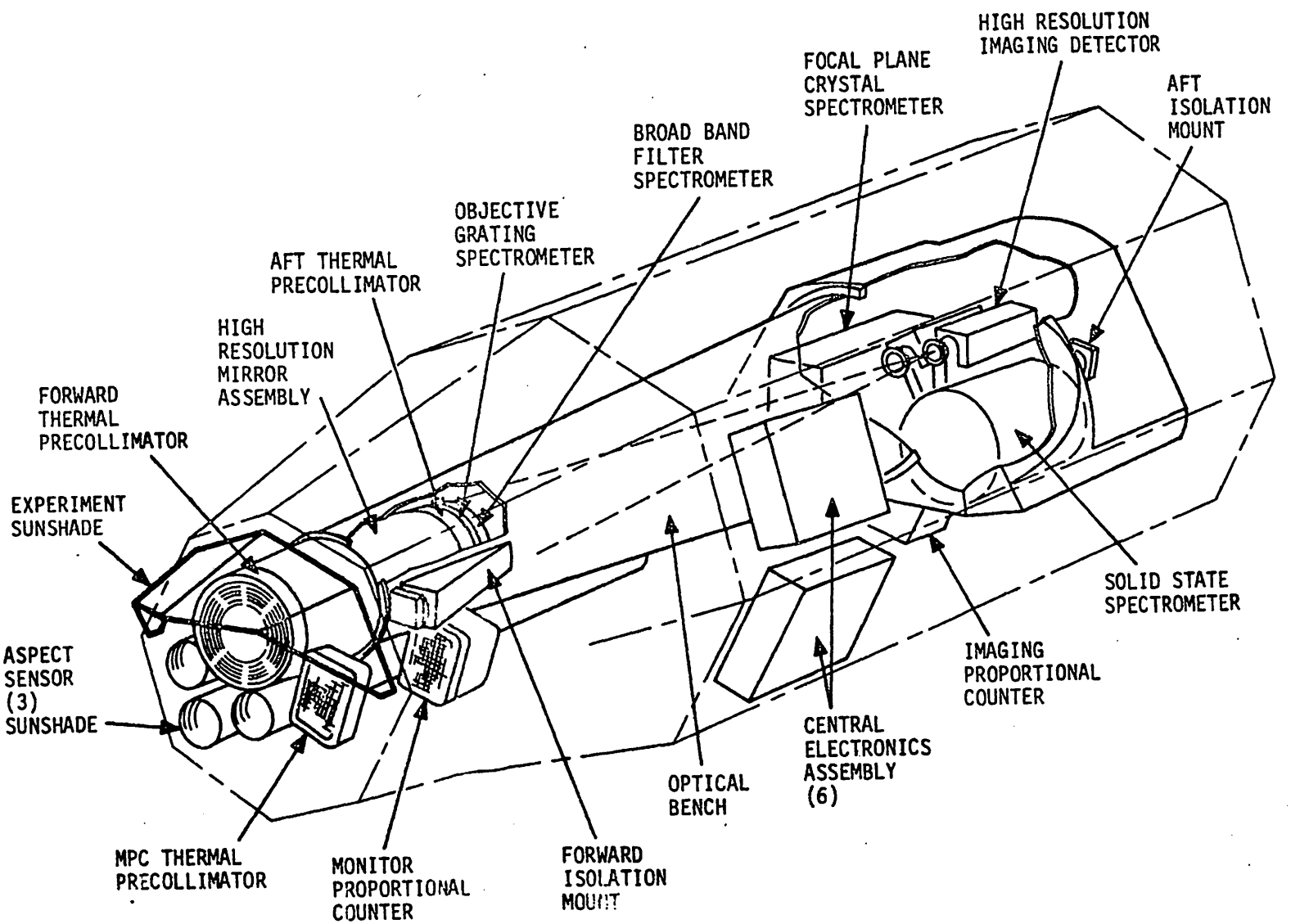

Figure 1

TABLE 1

HEAO-B INSTRUMENT PARAMETERS SUMMARY

Instrument	Field of View	Spatial Resolution	Effective Area	Energy Resolution (E/ΔE) (Range)	Time Resolution	Background
High Resolution Imager	25' Diam.	2" within 5' of axis (determined by mirror response)	~ 20 cm^2 at $\frac{1}{4}$ keV ~ 10 cm^2 at 1 keV ~ 5 cm^2 at 2 keV	3 color w/BBFS* 50-10 w/OGS** (0.15-3.0 keV)	8 μsec	5×10^{-3} cts/ $arcmin^2$-sec
Imaging Proportional Counter	75' x 75'	1'	~ 100 cm^2	0.7 at $\frac{1}{4}$ keV 3-4 at 1.5-4 keV (0.15-4.0 keV)	63 μsec	3×10^{-3} cts/ $arcmin^2$-sec
Solid State Spectrometer	6' Diam.		200 cm^2	3-25 (0.4-4.0 keV)	2 μsec - 5 msec	10^{-2}cts/sec
Focal Plane Crystal Spectrometer	6' Diam. 1' x 20' 2' x 20' 3' x 30'		1 cm^2 at E < .28 keV 0.1-1 cm^2 at E > .28 keV	50-100, E < 0.4 keV 100-1000, E > 0.4 keV	8 μsec	5×10^{-3} cts/sec
Monitor Proportional Counter	1.5^o x 1.5^o FWFM Collimated		600 cm^2	5 at 6 keV (1.5-20 keV)	1 μsec for Δt < 64 μsec Δt/100 for Δt > 64 μsec	10 cts/sec

* BBFS = Broad-Band Filter Spectrometer

** OGS = Objective Grating Spectrometer

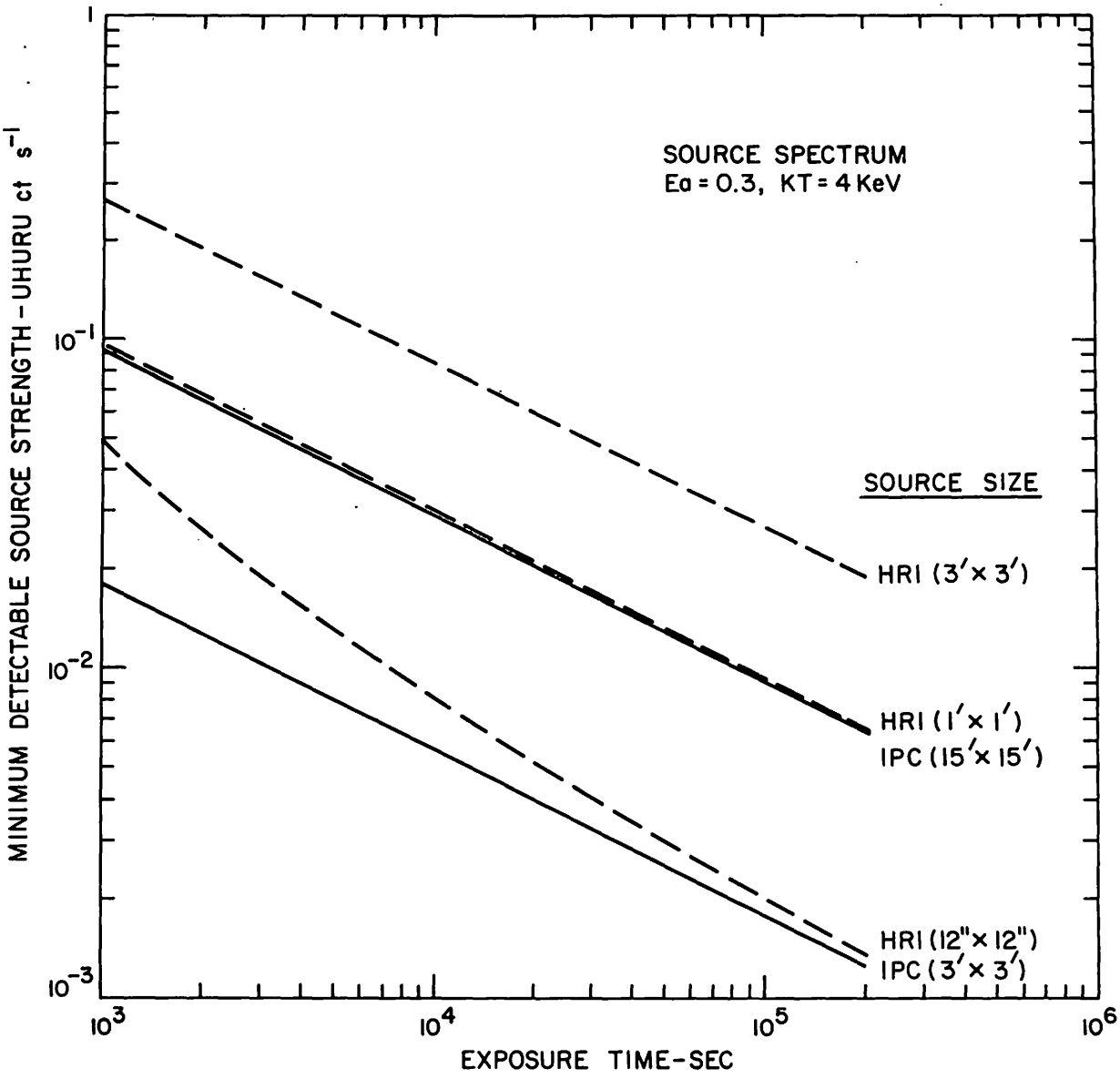

Figure 2. Sensitivity of HEAO-B Imaging Instruments

A. High Resolution Mirror

The telescope design chosen for HEAO-B is the Wolter type I geometry shown in Figure 3 in which the first element is a paraboloid and the second element is a confocal, coaxial hyperboloid. Axial rays are reflected towards the common focus by the paraboloid and then reflected by the hyperboloid towards its other focus.

The grazing angle required for efficient X-ray reflection is about one degree, and the optical elements have the appearance of shallow cones with relatively small ratios of collecting to polished area. The area cannot be increased indefinitely by increasing the length without a loss of resolution for off-axis rays, since the size of the image is approximately proportional to the length of the telescope. The area can be increased by nesting surfaces which have the same focal plane; this results in increased area and acceptable resolution since the individual mirror lengths do not become excessive.

The HEAO-B mirror design consists of four nested surfaces with optical diameters varying between 12.8 and 22 inches. The separation between the paraboloid-hyperboloid intersection plane and the focal plane is 135 inches, which results in a focal plane scale of 1 mm/arcminute, or 16.6 μ/arcsecond. The 21-inch segment lengths theoretically result in one arcsecond blur circle radii for sources within three arcminutes of the telescope axis. The accuracies achieved during the mirror fabrication degraded this to about 2 arcseconds rms radius, although the central peak of the response function is sufficiently narrow for arc second studies of high contrast features. Some calibration data and the theoretical rms blur circle radius are shown in Figure 4. Data points are the measured half width at half maximum (HWHM) at 44A and the radius containing 1/2 the X-ray flux incident at the focal plane. This "half-power" radius has been used to calculate the detectability of faint sources. The HWHM radius is the size of the high resolution core of the image and indicates the resolution that can be obtained for typical sources.

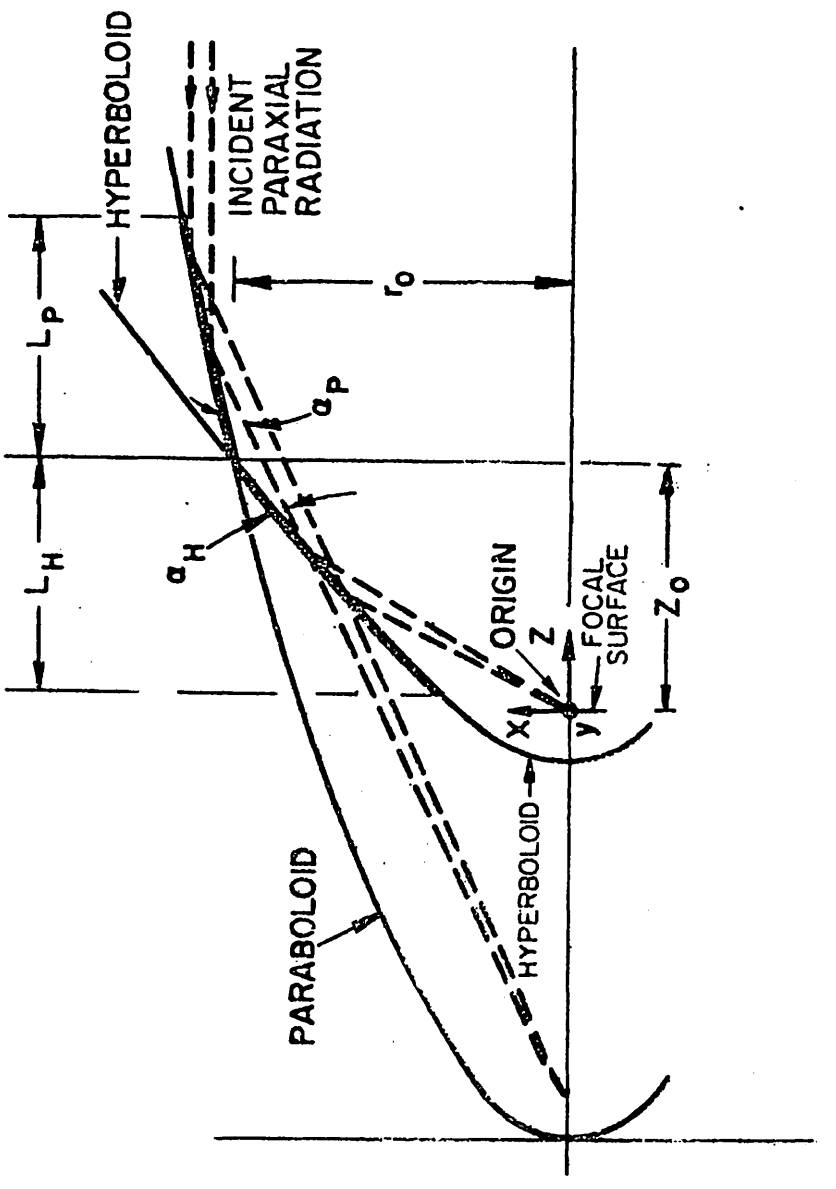

Figure 3 Wolter type 1 X-ray telescope geometry.

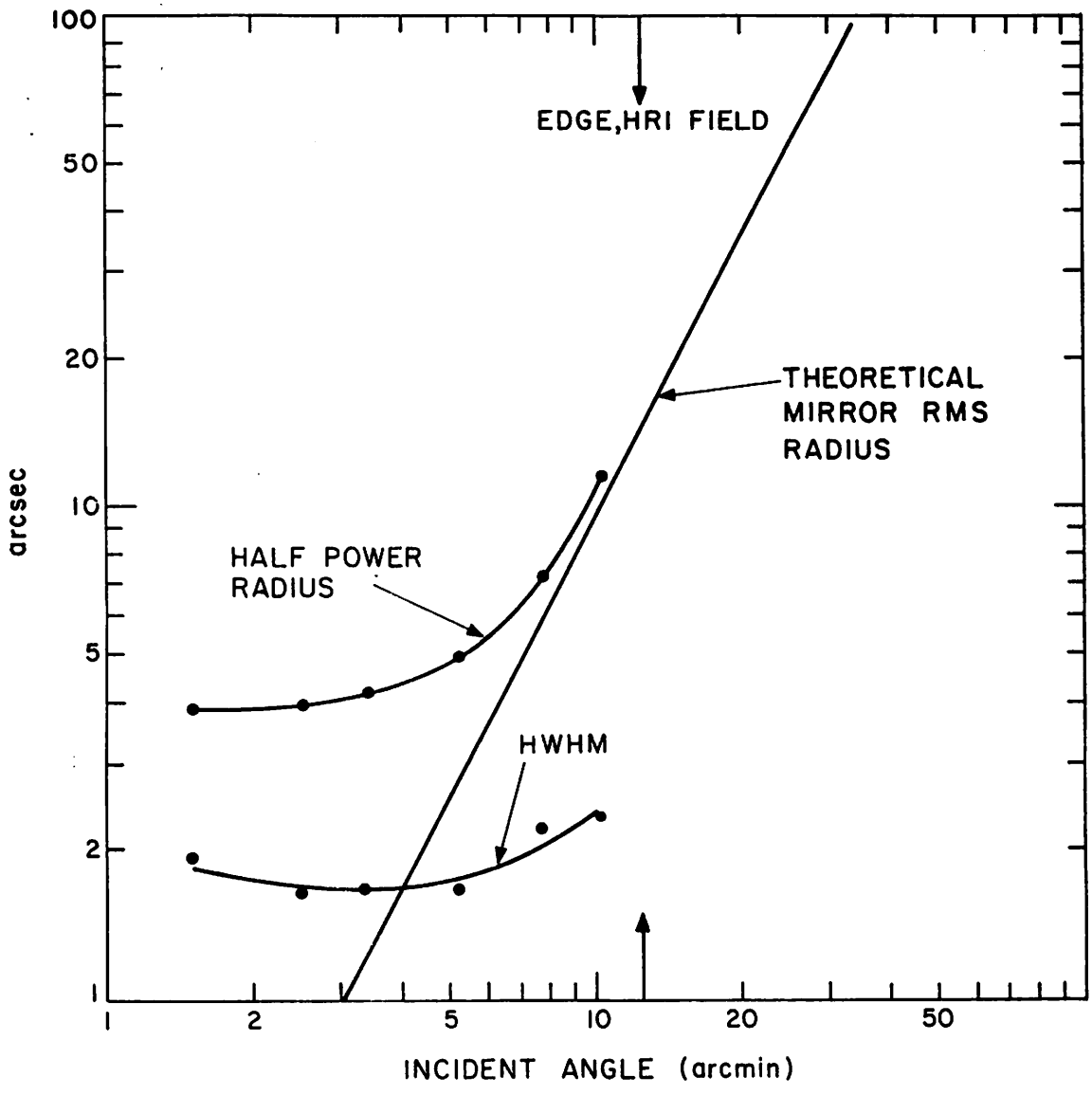

Figure 4. Measured HEAO-B mirror/HRI system response at 44Å.

The theoretical effective mirror area of the final design ranges from about 400 cm^2 at 0.25 keV down to about 30 cm^2 at 4 keV. The effective area includes the effects of the telescope geometry, and apertures which have been added to exclude unwanted rays from the portion of the focal plane within 20 arcminutes of the optical axis. Unwanted rays from off-axis sources could strike the focal plane without having reflected from both the paraboloid and the hyperboloid if the aperture stops were not present. The scattering loss due to surface roughness from a pixel 12 arcsec in diameter is 0.4 for energies of less than 1 keV, and rises to 0.7 at 4 keV. The effective mirror area folded with the detector responses will be shown in the following sections.

B. Aspect System

The experiment aspect system consists of three image dissector star trackers with sunshades, two protective bright object detectors, and a calibration light assembly. The system is used to update an onboard gyro reference for active spacecraft pointing (see Section IVb) and allows post-facto definitive aspect determination to about 1".

Each star tracker has a 2° x 2° square field of view; one is coaligned with the experiment pointing axis, the other two are offset about 2° in opposite directions. They are sensitive to stars brighter than 9th magnitude, with commandable magnitude thresholds. The intensity and rectangular coordinates of stars tracked by the three sensors are inserted in the telemetry each minor frame (0.320 sec).

There is also a calibration light system for in-flight referencing of the active focal plane instrument position to the aspect system. Three fiducial lights are mounted on each instrument except the SSS; suitable optics project the fiducial light images onto the three star trackers. Fiducial calibrations will be performed routinely as part of the planned observing sequences.

Aspect data will be reduced at SAO for the Consortium and Guest Observers. The fiducial calibration results will be included in the resulting aspect solution which will include pointing direction and roll angle as a function of time.

C. High Resolution Imager (HRI)

The HRI is a digital X-ray camera which provides high spatial and temporal resolution over the central 25 arcmin of the HEAO-B focal plane. The instrument has no inherent spectral resolution, but spectral studies can be performed using interchangeable broad band filters and the objective grating.

The HRI is composed of two microchannel plates (MCPs) operating in cascade, a crossed-grid charge detector (CGCD) and a set of electronics. An X-ray photon incident on the MgF_2 coating on the front of the first MCP produces an electron which is amplified in the first and second MCPs with a result that a burst of about 5×10^7 electrons is ejected from the back of the second MCP. Due to the nature of the MCPs this burst of electrons occurs at the same location and time (to within a few nanoseconds) as that of the X-ray photon. The burst of electrons is collected by the CGCD which is made of two orthogonal planes of wires. The position and time of the event is determined by the processing electronics and inserted into the telemetry stream with a limit of 100 cts/s.

A UV calibration system is provided for the determination of spatial resolution, spatial scale, and detector gain. This calibration lasts about 5 minutes and will be performed as part of planned observations as often as necessary -- possibly once per day when the HRI is in use. There is also an α-particle flouresced X-ray source providing X-rays at 1.5 keV which will be used for relative efficiency calibration on the ground and (rarely) in flight. The HEAO-B Observatory is equipped with three HRI detectors which are identical except for the material used for the UV opaque shields (cf, Table 2).

HRI performance and sensitivity factors are given in Tables 2 and 3. The effective area of the HRI-mirror combination is shown in Figure 5.

Shown in Appendix B Table 1a are total counting rates (counts/sec, 0.1-6.0 keV) expected from the HRI for various source spectra with unit normalization. Thus, for an HRI observation of the Crab (with no filter), with assumed spectrum of

$$\frac{dn}{dE} = 10E^{-2} \exp\left\{-\left(\frac{0.5}{E}\right)^{8/3}\right\} \text{ photons/keV-sec}$$

Table 1a of Appendix B indicates a predicted counting rate of 10 x 13.1 = 131 counts/sec.

TABLE 2

HRI Performance Parameters

(a) Spatial resolution* (detector only)	1 arcsecond (1σ, assumed Gaussian point spread) at all energies over central 25 arcmin diameter FOV. Twelve bits per coordinate.
(b) Energy resolution	None
(c) Temporal resolution	7.8125 μs
(d) Count rate capacity	Limited by telemetry to 100 per second. Additional events counted but not analyzed for position and time.

*The overall system performance is limited by the mirror resolution discussed in Section A, and shown in Figure 4.

TABLE 3

HRI Sensitivity Parameters

(a) UV shield material	1.00 μm Parylene N + .046 μm Al (Detector #2) 0.72 μm Parylene N + .054 μm Al (Detector #3) Detector #1 - to be determined - probably close to Detector #2
(b) Photocathode material	MgF_2
(c) Non-X-ray background	5×10^{-3} counts $(arcmin)^{-2} s^{-1}$ expected in-orbit rate.
(d) Sensitivity	1 count s^{-1} per 7 UFU or 1 count s^{-1} per 3×10^{-10} erg cm^{-2} s^{-1} (0.1 - 4 keV, Crab spectrum).

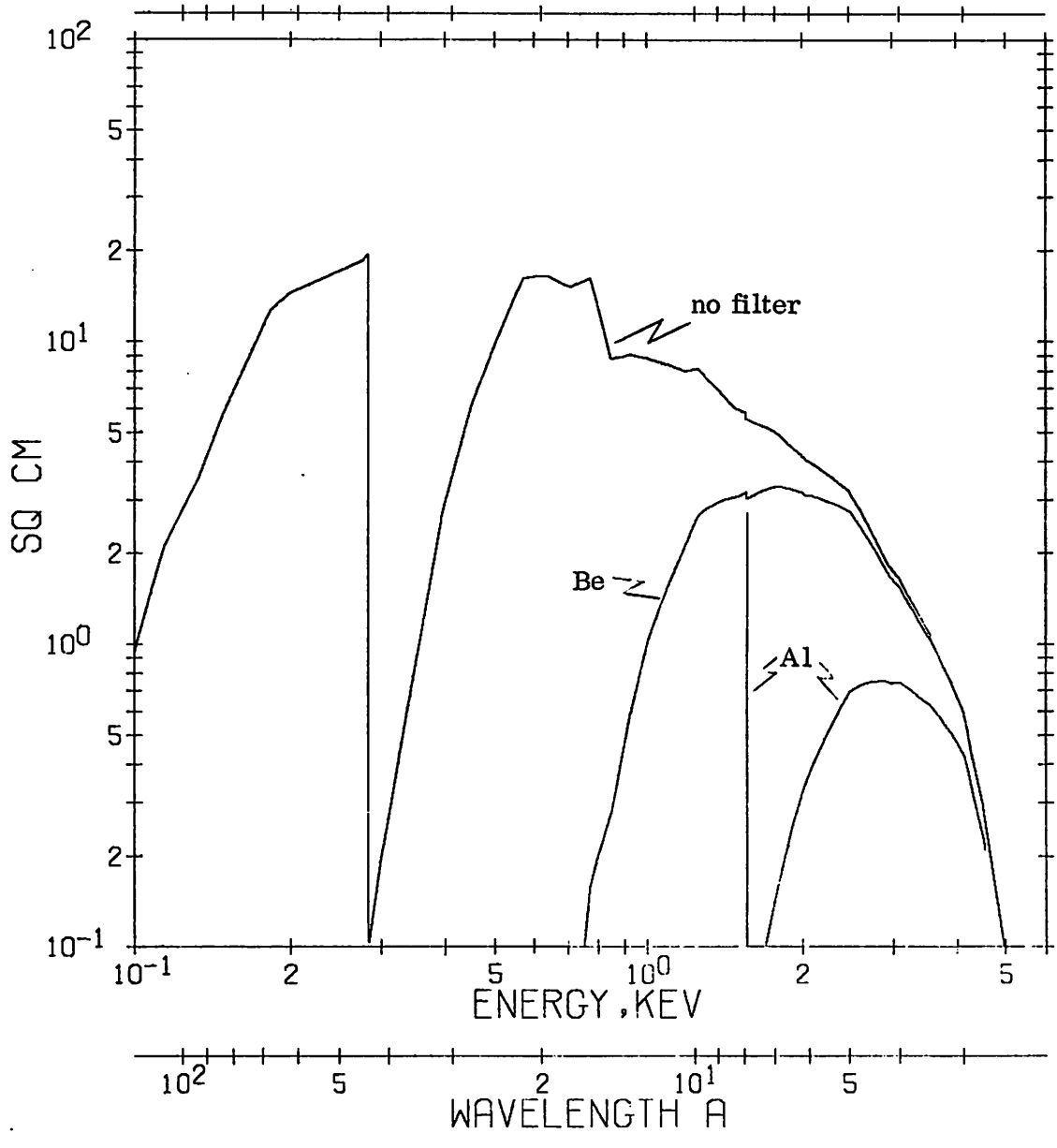

Figure 5. Effective area HRI #2 with no filters, with Be fliter, and with Al filter. Photons which scatter from the mirror with angles greater than 6" have not been included, thus this efficiency is for 12" pixels.

D. Broad Band Filter Spectrometer (BBFS)

The filter spectrometer will be used with the high resolution imager (and possibly the imaging proportional counter) to extend the spectral resolution. This will be particularly useful for studying detailed features, high source density regions, extended sources, and sources too weak to be studied with the high spectral resolution instruments. The instrument consists of two filters, either or both of which can be placed on command into the converging X-ray beam from the telescope. The mechanism is located near the mirror to avoid a correlation between filter transmission and focal plane position.

The filters which have been selected are 1 mg/cm^2 of aluminum and 2 mg/cm^2 of beryllium. Each has been coated with $\sim 5\mu$ of parylene. The transmission of these filters folded with the mirror effective area and the HRI efficiency is shown in Figure 5. The filters enable the incident spectrum to be divided roughly into the bands $E < 1.25$, $0.8 < E < 1.5$, and $E > 1.5$ keV. Total counting rates expected for various source spectra with unit normalization are included in Appendix B, Tables 1b and 1c.

E. Objective Grating Spectrometer (OGS)

The OGS consists of two transmission gratings, either of which may be placed into the X-ray optical path at the exit from the High Resolution Mirror. The High Resolution Imager usually will be used to detect the diffracted images. The gratings used in HEAO-B were prepared by Dr. Jan Dijkstra and his colleagues at Utrecht. These gratings consist of gold lines about 0.2 μ thick and 0.5 μ wide separated by open spaces of the same width. The fine lines are supported by a random pattern of larger gold lines. Grating spacings of 500 and 1000 ℓp/mm have been selected, resulting in the following characteristics:

	500 ℓp/mm	1000 ℓp/mm
Dispersion (Å/arcsec on HRI)	0.129	0.063
Range, HRI center on axis, 1st order	0 - 101 Å	0 - 49 Å
Range, HRI edge on axis, 1st order	0 - 202 Å	0 - 99 Å

The grating resolution is limited by telescope resolution at shorter wavelengths. The resolution at wavelengths longer than 12 Å (23 Å) is limited by aberrations using the 500 ℓp/mm (1000 ℓp/mm) grating. For these longer wavelengths, the resolution is about $\lambda/50$.

The area of the gratings, using the HRI detector, are shown in Figures 6 and 7; total counting rates expected for various source spectra with normalization are included in Appendix B, Table 1d and 1e. The sensitivity for a narrow line emission feature can be calculated using the efficiencies in Figures 6 and 7 and the HRI detector background data.

The 1000 line grating has been strengthened by coating with 2.5 μm parylene. Also, below the carbon K edge, the dispersion is large and one first order falls outside the HRI sensitive area. The calculated curve of Figure 7 includes this effect.

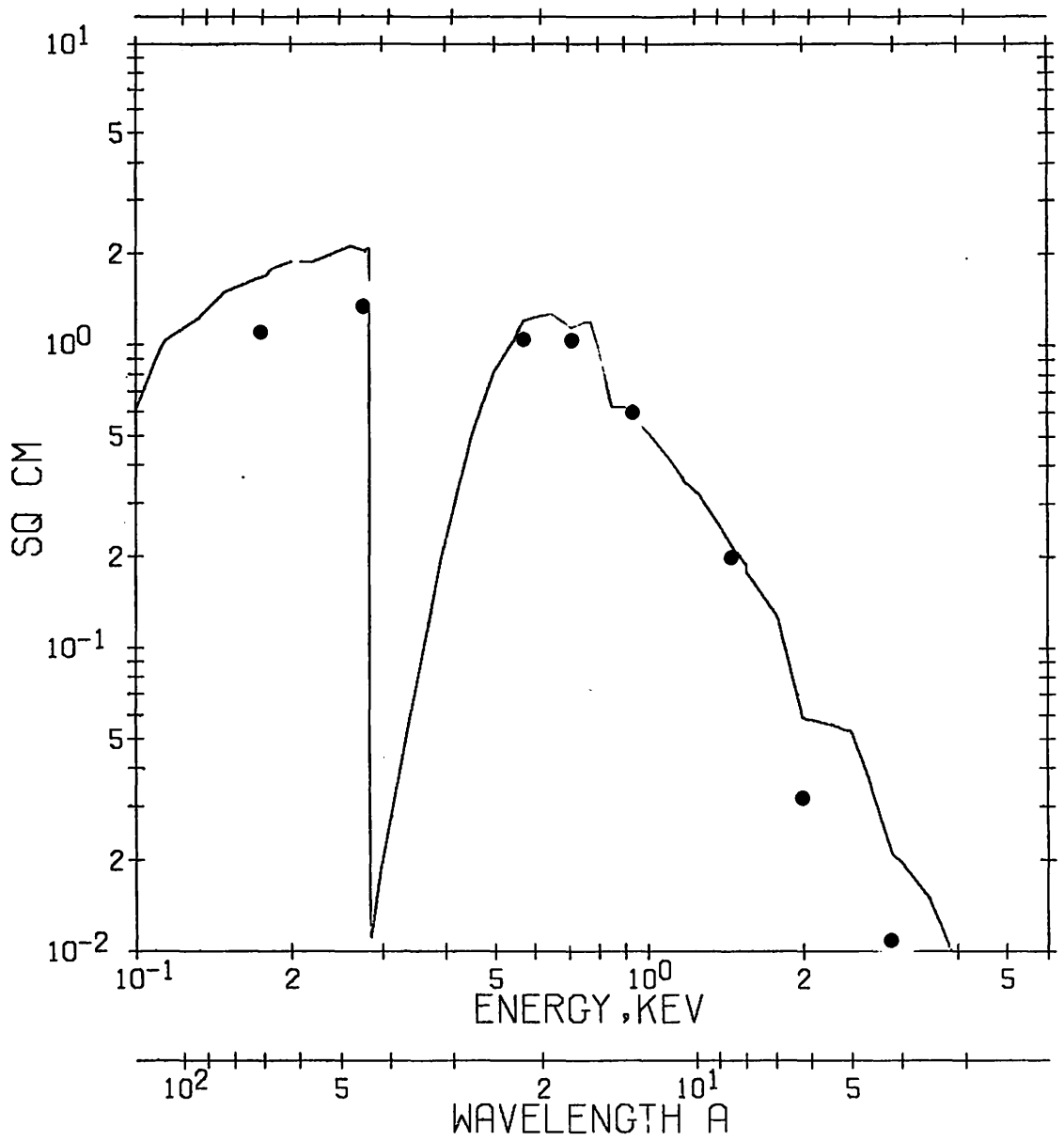

Figure 6. HRI-OGS Effective Area 500 line/mm Grating. Solid line is theoretical prediction, points are calibration data.

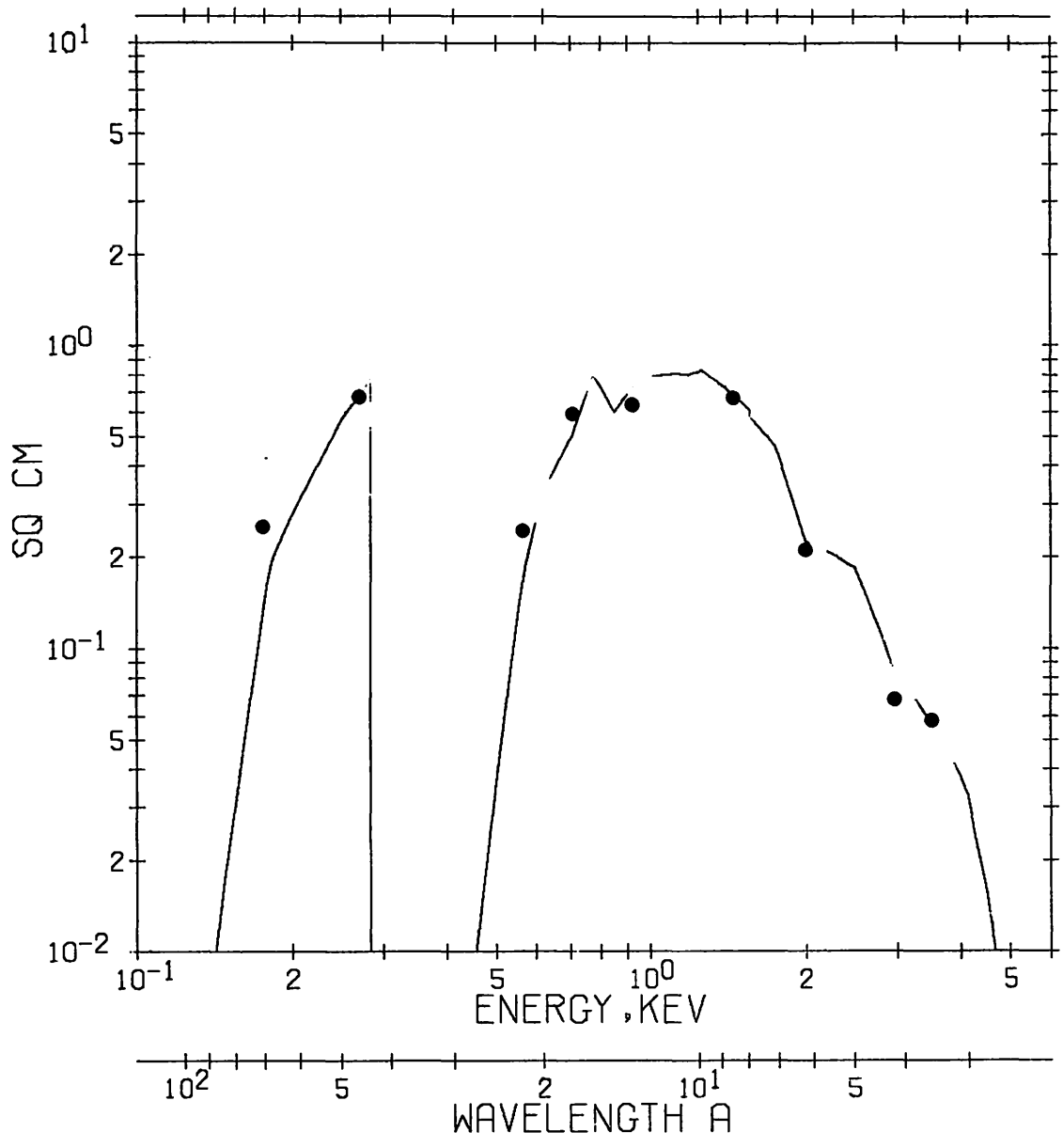

Figure 7. HRI-OGS Effective Area 1,000 line/mm Grating. Solid line is theoretical prediction, points are calibration data.

F. Imaging Proportional Counter (IPC)

The IPC is a position sensitive proportional counter which provides the HEAO-B Observatory with good efficiency and full focal plane coverage, together with moderate spatial and spectral resolution. Included in the HEAO-B Observatory are two such assemblies, identical except for the material used for the entrance window (see Table 4).

An in-flight calibration system produces α-particle fluoresced X-rays at 0.28, 1.5 and 4.6 keV for determining relative detector gain. The system will be commanded on for periods of up to 5 minutes during IPC operation as necessary.

The counter body houses the electrodes in a density-regulated gas mixture (see Table 4). The composition of the gas is passively maintained by the use of a controlled leak located in the vacuum box.

The IPC electrodes consist of an anode centered between two cathodes which receive induced signals from the avalanches occurring at the anode. Pulse rise time processing of the induced signals permits the determination of the Y-Z coordinates of events to a precision of 1 mm, which corresponds to 1 arcmin over a field of view of 60 x 60 arcmin. The centroid of the signal from a point source can be determined to better than 1 arc min. A gas gain of $\sim 10^5$ is required to achieve this resolution and is obtained by operating the anode and cathodes (which are separated by 3 mm) at potentials of 3600 and 900 volts, respectively. Processing of anode signals (event timing and pulse height analysis) provides 63 μsec time resolution and 32 energy channels in the range from 0.1 to 4.5 keV.

Located within the same counter body below the IPC electrodes and covering the same area is a background counter, the signals from which are used in anticoincidence to

provide background rejection for the IPC.

IPC performance and efficiency factors are given in Tables 4 and 5. The effective area of the IPC-mirror combination (for both detectors) is shown in Figures 8 and 9. Appendix B, Tables 2a-f show counting rates (count/sec, 0.1 - 6 keV) for the two IPC detectors, (and with BBFS filters) for trial source spectra with unit normalization. Thus, for the Crab, the IPC would observe a total counting rate of 1162 or 763 cts/s (limited to 125 cts/s by the telemetry), depending on the detector used (see Appendix B, Tables 2a and 2d).

TABLE 4

IPC Efficiency Parameters

(a) Entrance window	77% transmissive mesh
	0.2 μm carbon dag
	2 μm polypropylene, det. A
	0.4 μm lexan, det. A
	3 μm mylar, det. B
(b) Absorbing gas	800 torr, STP
	4 cm deep
	Composition
	Argon 84 %
	Xenon 6 %
	CO_2 10 %
(c) Active area	7.62 x 7.62 cm, total window
	3.8 x 3.8 cm, unobstructed area
(d) Sensitivity	1 count sec^{-1} per UFU or
	1 count sec^{-1} per 4 x 10^{-11} erg cm^{-2} sec^{-1}
	(0.1 - 4 keV, Crab spectrum)
	see Appendix B2
(e) Non-X-ray background	1.5 x 10^{-3} counts $mm^{-2}sec^{-1}$, 0.1-1.5 keV
	1.5 x 10^{-3} counts $mm^{-2}sec^{-1}$, 1.5-4 keV

TABLE 5

IPC Performance Parameters

(a) Spatial resolution*:	1 arcmin, 1.5 keV and above 2 arcmin, 0.28 keV 10 bits per coordinate
(b) Energy resolution (32 channel PHA)	$\leq$ 50% FWHM, 1.5 keV and above 140% FWHM, 0.28 keV
(c) Temporal resolution	63 μ seconds
(d) Count rate capacity	125 per second, telemetry limit
(e) Background rejection	background counter provides anticoincidence veto signal

*2σ of an assumed Gaussian point-spread function.

The resolution becomes limited by the mirror performance at the edges of the field of view, see Figure 4.

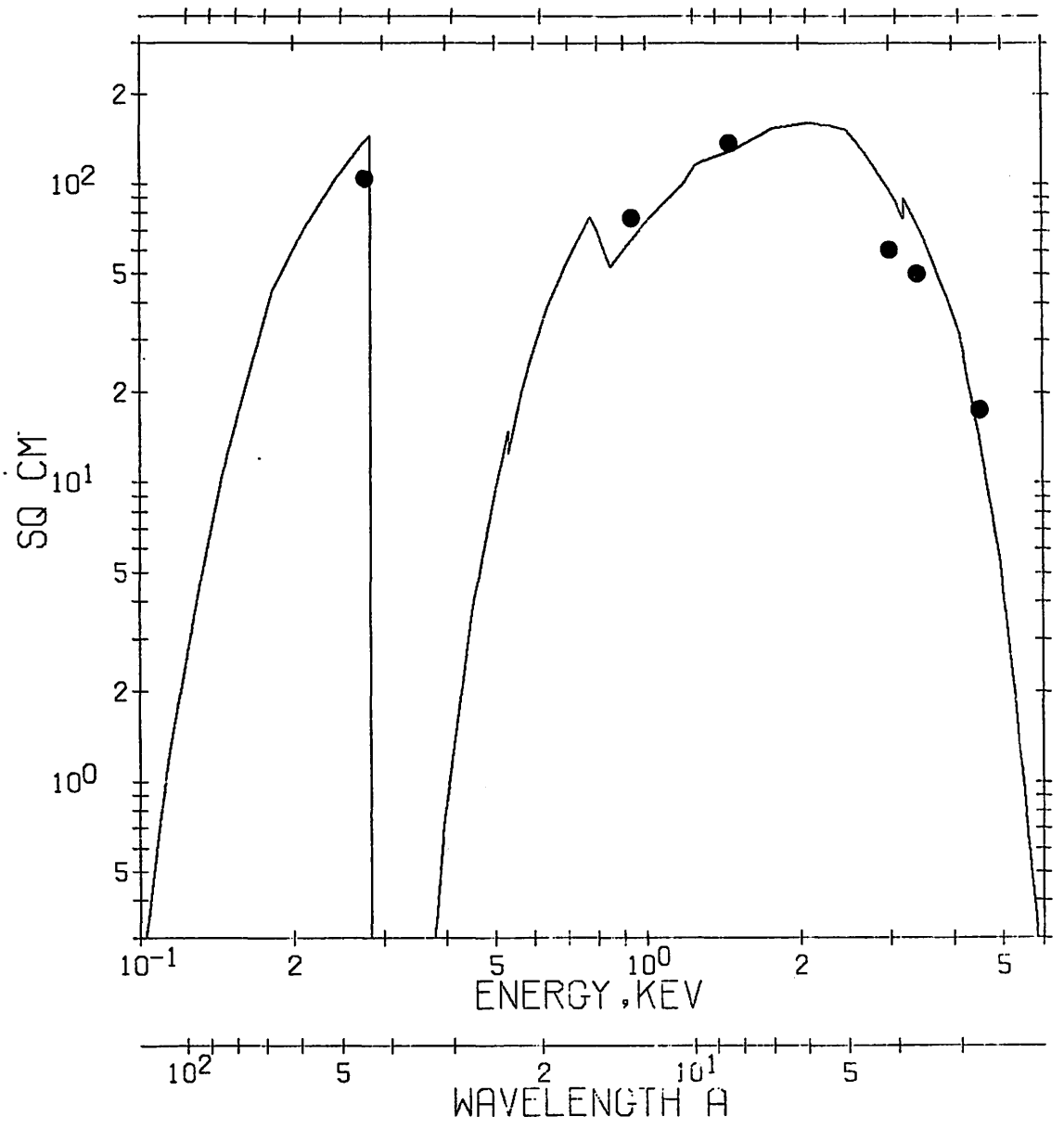

Figure 8. Theoretical effective area of IPC-A. Points are calibration data.

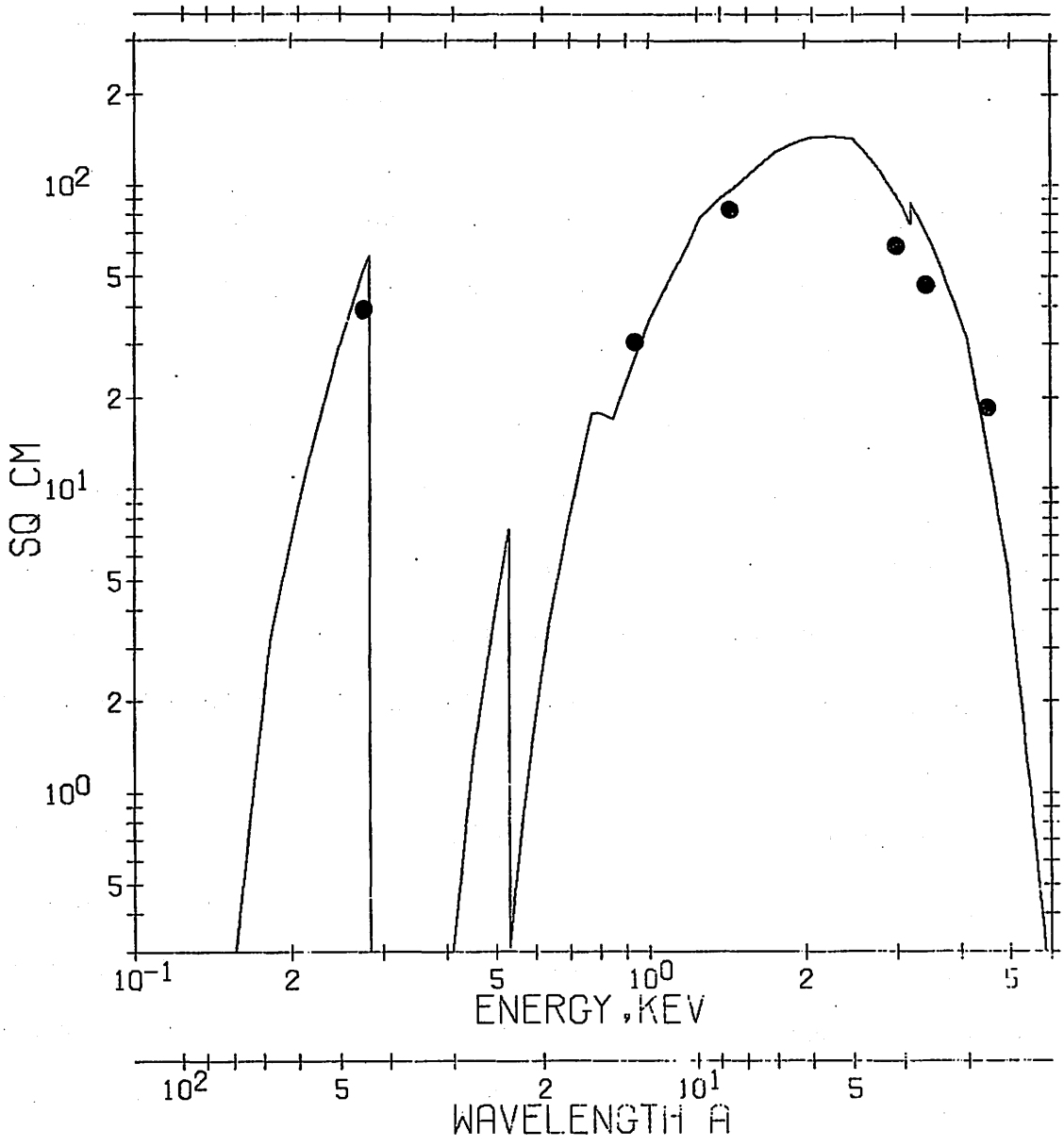

Figure 9. Theoretical effective area of IPC-B. Points are calibration data.

G. Focal Plane Crystal Spectrometer (FPCS)

The FPCS is a curved crystal Bragg spectrometer. The X-rays from a celestial source are focused by the HEAO-B telescope and pass through an aperture/filter wheel assembly located at the focal plane. They diverge in an annular cone with half angles of 2.°5 to 5° and strike a curved diffractor. X-rays of appropriate wavelength to satisfy the Bragg condition are reflected and detected with an imaging proportional counter. There are six diffractors available.

The FPCS can be operated as a conventional curved crystal spectrometer or used in a modified fashion to achieve higher resolution. In both cases the curvature of the diffractors serves the primary purpose of intercepting the incident X-rays at nearly constant Bragg angle despite the large angular divergence of the beam. In order to achieve this benefit, the relative positions of the diffractor and the point in the focal plane from which the X-ray beam diverges must be maintained so that each lies on the circumference of a circle (the Rowland circle) with a diameter equal to the radius of curvature of the diffractor lattice. As the Bragg angle is changed, the relative positions of the diffractor and focal plane must also be changed.

When operated as a conventional curved crystal spectrometer, the detector is positioned so that it also lies on the Rowland circle. The diffracted X-ray beam is refocused at this location to form an astigmatic image of the X-ray distribution in the telescope focal plane. A source, such as an X-ray star, which appears as a point in the focal plane is imaged at the FPCS detector as a slightly curved line perpendicular to the plane of the spectrometer and to the anodes of the imaging proportional counter. Thus, the effective detector area, defined ex post facto on the ground, is typically less than 1 cm^2, so the non-

X-ray background is small.

A particular spectral feature is studied by scanning a narrow range of crystal angle (and therefore of wavelength) with all other elements held fixed -- the deviation from ideal Rowland circle geometry during such a scan is small. In flight the uncertainty in the HEAO-B spacecraft attitude (± 1 arcmin) introduces an uncertainty of ~ 10 to 20 arcminutes in the Bragg angle predicted at a particular crystal setting. The crystal scan is sufficient to allow for this uncertainty, which is then removed during analysis by using the star camera aspect data which are accurate to ~ 1 arcsecond.

The imaging property of the spectrometer and detector allows study of extended sources such as supernova remnants. These can be observed through one of four (3 x 30, 2 x 20, 1 x 20 arcmin and 6 arcmin diameter) apertures. The position of arrival of an X-ray at the detector is a function of both wavelength and position in the source. This function can be partially deconvoluted to yield both spectral and spatial information.

When operated in the conventional manner, the FPCS will achieve its highest sensitivity, but will generally be limited in resolution by the geometric effects of the diffractor curvature. These typically give a Bragg angle spread of 2 to 20 arcminutes depending on the angle. For extended sources the resolution is further limited by the imaging capabilities of the detector.

For the study of point sources it is possible to improve the spectral resolution by departing from the conventional Rowland circle configuration. In this mode the detector is located closer to the diffractor so that the reflected X-rays are intercepted before they converge to the usual line image. The position of arrival of each X-ray photon at the detector is then related by geometry to the point on the diffractor at which it was reflected and,

therefore, to its angle of incidence and its wavelength. In effect, the dispersion of the curved diffractor is utilized to improve the spectrometer resolution at the expense of a larger effective area at the detector and thus a higher non-X-ray background. With the spectrometer operated in this defocused mode, the geometrical contribution to the angular resolution is still a function of Bragg angle but is always ≤ 5 arcminutes. For many settings, the inherent resolution of the diffractor will dominate.

The motions for both conventional and defocused spectrometer operation are performed with a mechanical assembly driven by stepping motors. Four motors are used to adjust independently the diffractors and detector angles and the linear positions of diffractor and detector. A fifth motor is used to select any one of six diffractors mounted on a turret assembly, and a sixth controls the aperture/filter wheel. The positions of all the moving elements are monitored with potentiometer readouts.

The stearate and laurate multilayers are toroidal, and the rest are composed of cylindrical facets mounted in a quasi-toroidal configuration.

The detector is a multi-anode, position-sensitive proportional counter. In order to allow operation of the FPCS in the "unfocussed mode" and to permit the study of extended sources, the detector uses resistive anodes. It has $\sim$ 1 mm resolution along a direction parallel to the plane of the spectrometer and 1 cm (wire to wire) resolution along the orthogonal direction. Anticoincidence anodes are located on three sides of the active volume and are used to reject non-X-ray events.

The counter window is stretched polypropylene film dipped in a Formvar solution to reduce the leak rate of the counter gas. The gas is a mixture of argon, xenon and carbon dioxide (84:6:10). Sufficient gas is carried on board to permit operation of the detector as a flow counter, thus avoiding problems due to changes in gas composition due to differential leakage through the window. Two identical counters provide redundancy. An on-board Fe^{55} calibration source can be made to illuminate a narrow strip on the detector. The counter high voltage is adjusted to obtain appropriate gain for the energy region of interest.

Ground calibration of the spectrometer throughput has been made at several discrete wavelengths. In-flight calibration consists of two fluorescent X-ray line sources which can illuminate the crystals with Na K, and C K X-rays, and a filter which can introduce an Al K, Cu L, Cr L or Zr L edge into a bright continuum. In-flight throughput will be determined from bright continuum sources (e.g., Sco X-1).

The FPCS sensitivity is a complicated function of energy, continuum source strength, integration time and background. In Appendix C we list various parameters as functions of energy for 1000s and 10000s observations assuming nominal operating modes of the spectrometer. The minimum detectable line fluxes shown in the last four columns are for a known line detected with a confidence level corresponding to four sigma. The equivalent width in keV can be obtained by dividing such values by the continuum flux noted at the head of the corresponding column.

The resolution attainable is also a complicated function of spectrometer setting and operating mode. Appendix C lists under RES the approximate resolution $E/\Delta E$ obtained at the Rowland circle focus and is applicable to weak point sources. The improvement in resolution achieved forward of the Rowland circle for point sources is shown in Figure 10. For extended sources the maximum resolution is ~350.

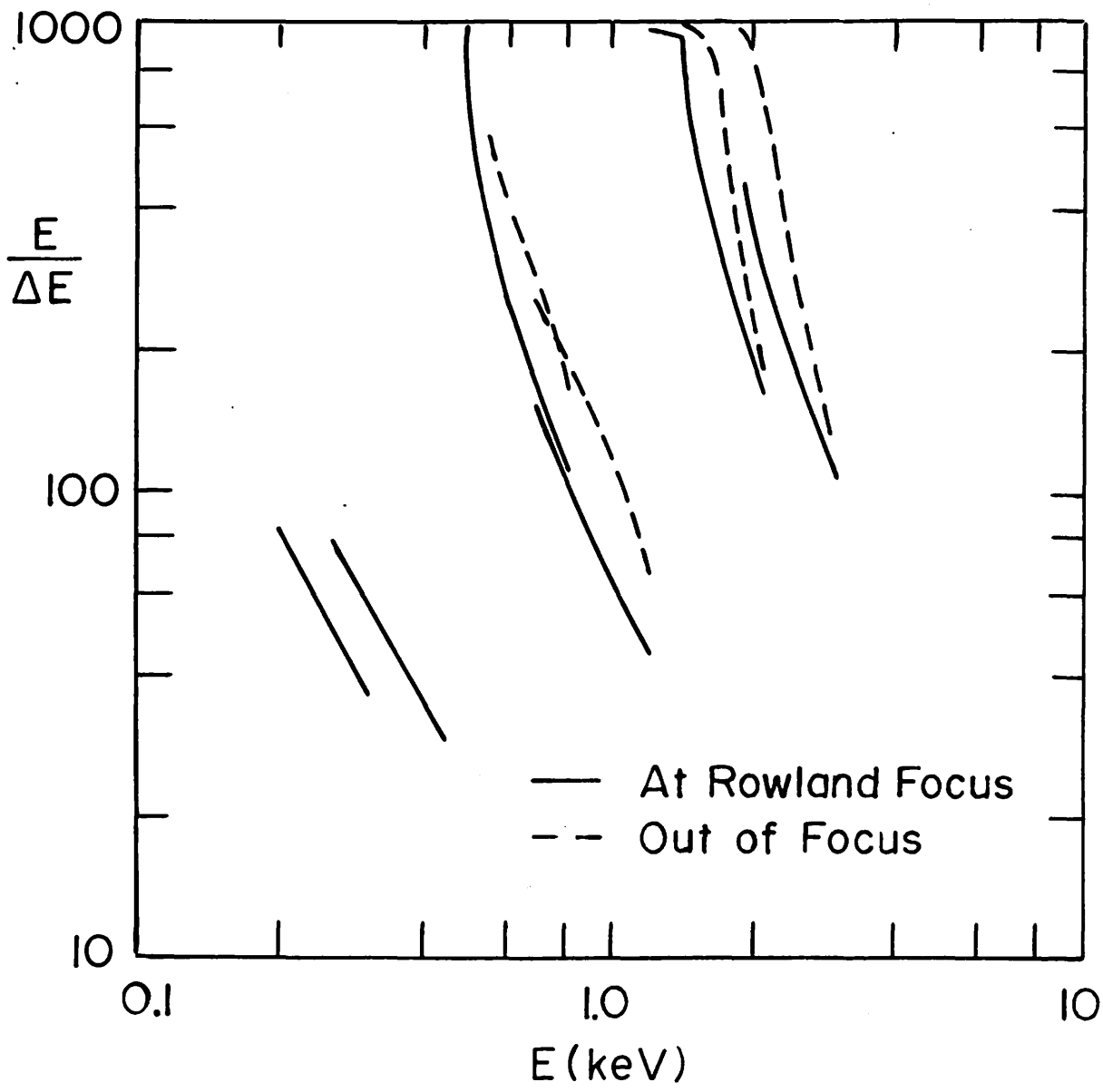

Figure 10. Estimated limiting FPCS resolution for normal operation (solid curves) and out-of-focus operation (dashed curves).

H. Solid State Spectrometer (SSS)

The Solid State Spectrometer (SSS) uses a Si(Li) crystal for the simultaneous observation of X-rays over the energy range 0.4 - 4.0 keV. This non-dispersive device offers a distinct improvement in resolving power over equivalent proportional counter techniques. The limiting FWHM resolution is $\approx$ 140 eV. The combination of the solid-state detector with the large collecting area of the Wolter Type I glancing incidence telescope, therefore, offers a powerful instrument for the observation of both spectral and temporal X-ray phenomena.

i. Experiment Description

The detector consists of a 9 mm diameter, 3 mm thick Si(Li) chip, which has two concentric grooves machined on the n-side or reverse of the crystal. The front face or the p-side of the crystal is deposited with a $\leq$ 100 Å thick gold contact. This contact is used to bias the central detector volume inside the innermost groove. It is observed that this gold layer is clumped and irregularly distributed on a scale of microns. The average transmission for soft X-rays of the detector front face is, therefore, smoothed by mounting the detector slightly out of the telescope focal plane to produce a resultant defocussing to a size of $< 1\ mm^2$. The other factors affecting the low energy performance of the instrument are the transmission of an aluminized parylene filter and the non-depleted region at the crystal p-side forward face. This region is arranged to be $\sim$0.1 microns in thickness over the approximately 6 mm diameter "entrance window" of the central portion of the detector. The resultant calculated detector efficiency is shown in Figure 11 and the convolution of this efficiency with the calculated telescope effective area as a function of energy is shown in Figure 12.

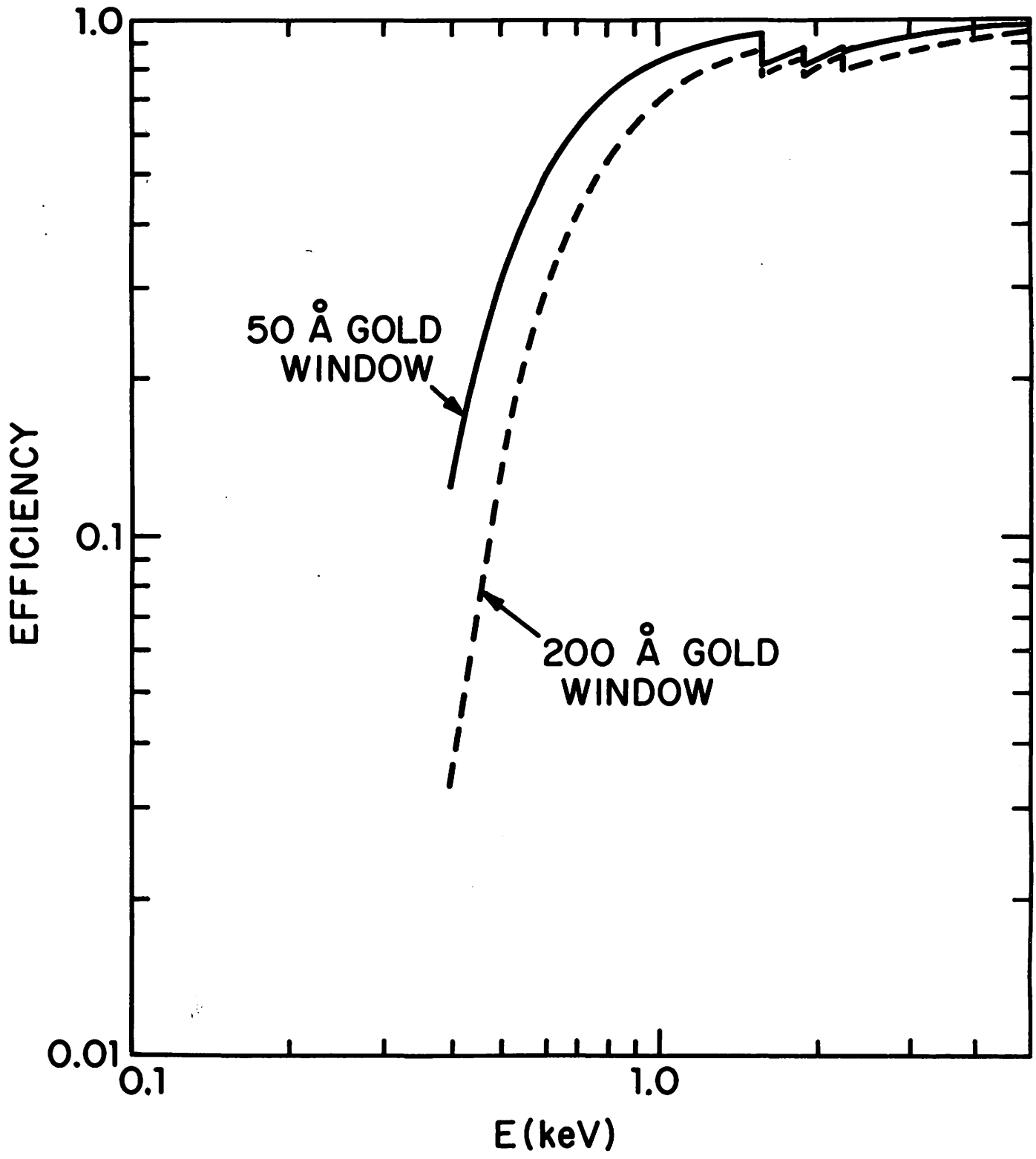

Figure 11. SSS Detector Efficiency

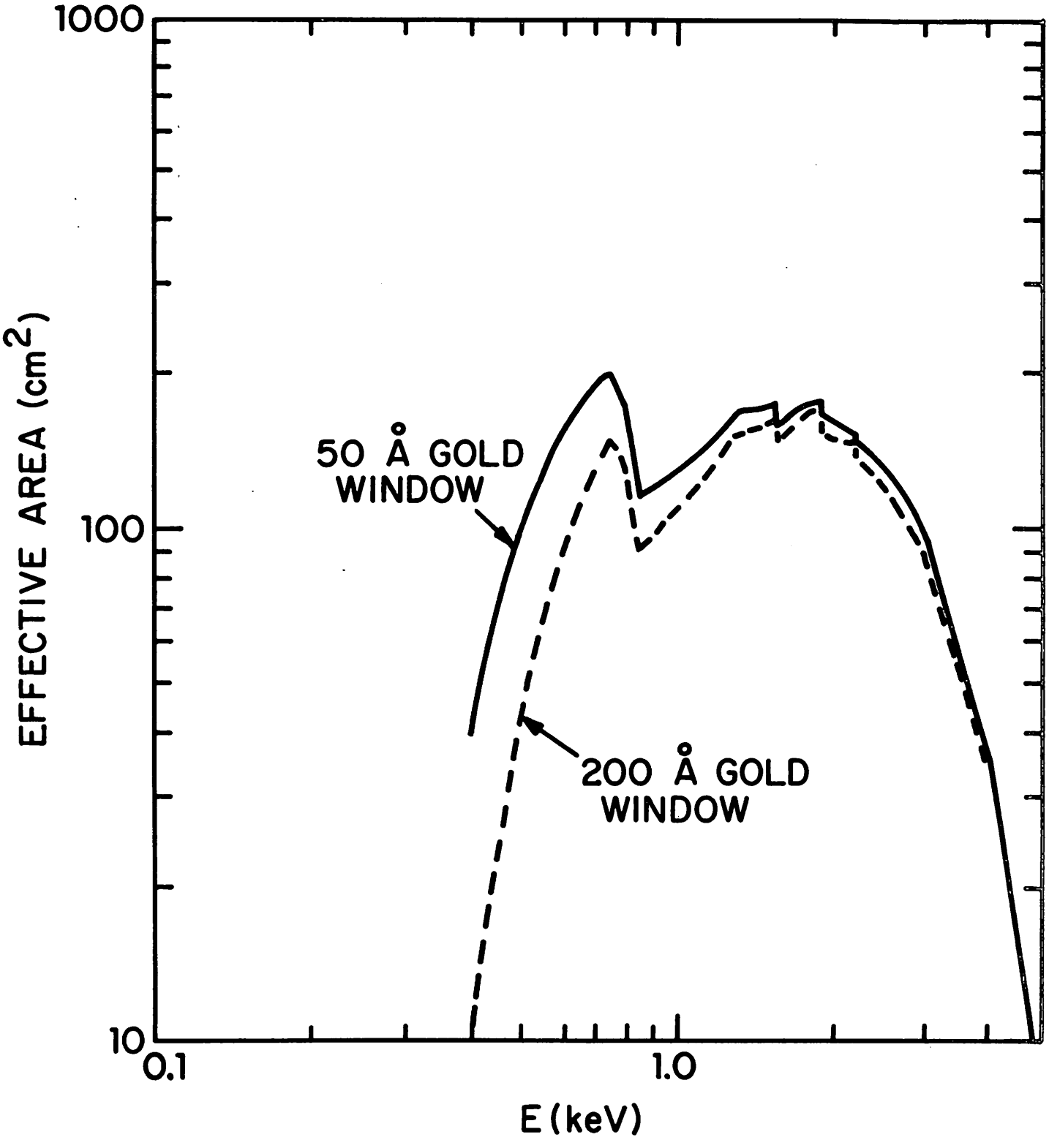

Figure 12. SSS Effective Area

The observed high energy cut-off is determined by the critical angle for glancing incidence X-ray reflection. A detector background of 10^{-2} counts/sec is expected.

Inclusion of the innermost groove provides a sharper edge to the central detector. A further Ge (HP) crystal is mounted behind this detector, and when operated in its normal anticoincidence mode with the central volume, acts as a "backstop" for the removal of events due to charged particles.

Opto-electronic feedback is used for the Si(Li) detector charge amplifier, since this completely removes the noise contribution from a feedback resistance. This is especially important using the proposed time constants for this detector. The FET and LED for this feedback arrangement are mounted below and in the immediate proximity of the Si(Li) detector. The major contributions to the noise of this device result from the thermal noise generated in the FET conducting channel and to the inherent properties of the detector itself. The former noise source is inversely proportional to the square root of the filter time constant of the system. It is therefore necessary to use a time constant of $\gtrsim 10$ μsec to obtain a resolution approaching the limiting value of 140 eV for spectral analysis and values of 5.7, 17.1, 28.5 and 40 μseconds are available on command. The actual value selected for an observation is determined by the expected counting rate, since pileup effects make the long time constants inappropriate at high count rates. A shorter time constant ($\sim$1 μsec) is required for absolute timing and for the anticoincidence logic, but the larger noise contribution to this channel demands a somewhat higher low-level discriminator. Electronic processing of the opto-electronic charge amplifier output is, therefore, made

concurrently through a fast amplifier and a longer time-constant system for spectral analysis in parallel. A similar arrangement is not required for the Ge "backstop," and therefore conventional resistive feedback charge amplifiers are employed with time constants of ~1 μsec on this system.

Two of the above detector assemblies are mounted in the common detector container of a solid Ammonia/Methane cryostat, which maintains the operating temperature of the solid state devices at approximately 100° K. Redundancy is provided since either of these detectors may be positioned in line with the telescope axis by command. The entrance apertures of the detectors are collimated mechanically by a parylene-coated aluminum baffle at 160° K to remove low energy X-rays generated by fluorescence in the cryostat, and this device also provides an effective cold trap for the detectors. Immediately above this collimator a thin window of aluminized parylene is employed to remove UV and optical radiation focussed by the telescope.

ii. Data Handling Modes

Three internal experiment operating modes are available; these are PHA, Δt and multiscaler (MS). In a standard observing sequence for a source all three modes would be used. In the PHA mode, pulse height analyzed data are stored in a 128-channel memory, which is read out every 1.28 seconds. In addition, data from the central detector are processed by the 1 μsec fast amplifier, discriminated and accumulated in an 8-bit counter, which is read out every 2.5 msecs. The Δt mode provides the highest resolution for the integrated time intervals between successive X-ray events. These intervals are measured with an accuracy of $^{+1}_{-0}$ μsec for events that are discriminated (i.e., > 2 μsec apart) and the values are stored in the 128-bar quasi-logarithmic histogram. The histogram is read out every 1.28 seconds. The remainder of the experiment data output is used to record the

central detector X-ray rates and PHA channel for the first event detected, each obtained in a 5 msec sample time.

The relative arrival times for the first (at most) 128 X-ray pulses, that are recorded by the Si central detector in each successive 640 msec time interval, are recorded in MS mode to an accuracy of $^{+5}_{-0}$ μsec for the initial 640 μsec of an interpulse interval and reducing to $^{+40}_{-0}$ μsec for the remainder of the interval. In addition, the Si central rates and PHA data are recorded as in the Δt mode, with sampling times of 10 msec and 5 msec, respectively. Six additional summary rates are recorded in all three operating modes. The total Si(Li) detector (before anticoincidence) counting rate is output twice per 1.28 secs. The remaining three rates are output once per 1.28 secs; these are the total Ge backstop counting rates, the number of times the opto-electronic LED feedback was activated and the system dead-time recorded as a multiple of 5 μsecs.

iii. Operation

Commands are provided for optimizing several experiment parameters. These include the voltage bias on the Si(Li) front face gold contact and Ge(HP) "backstop," the time constant adopted for the Si(Li) detector volume and the values of the low level discriminators (LLD) for the Si and Ge detectors. In addition, a very low level discriminator (VLLD) setting is used to extend the instrument energy range to its lowest limit. However, events which are recorded at these energies are not included in the experiment summary rates.

The instrument can be calibrated directly in orbit with the use of Fe^{55} k-capture X-ray sources. These sources are mounted on the underside of the cryostat vacuum cover, which may be rotated into position by command. In addition, a Test Pulse Generator (TPG) may be used to check out a variety of analog and digital electronic

functions. It is expected that these calibrations will be performed with each observation.

The most general observational sequence commences by testing the integrity of the aluminized parylene window against penetration by UV radiation, before performing an instrument calibration using the internal Fe^{55} source. An observation of the X-ray source of interest is made using one or more of the three experiment modes and then finally a comprehensive check-out of the instrument electronics is made with the TPG. It is not necessary for the SSS to be positioned at the focus of the telescope during the calibration and check-out phases of the above sequence, but there is a requirement for the SSS scientific telemetry format throughout. It is expected that a source observation will typically total 20-50 minutes duration.

I. Monitor Proportional Counter (MPC)

The Monitor Proportional Counter consists of a proportional counter viewing space through a collimator co-aligned to the high resolution telescope. The counter has a 1.5 mil beryllium window and two Ar-CO_2 gas volumes. The active area is 667 cm^2. The system has an X-ray collimator, a thermal impedance covering the spacecraft viewing aperture, and an in-flight calibration system. The counter has four anodes, each with a dedicated preamp and dedicated discriminators. A veto signal is generated if events are detected simultaneously on adjacent anodes. The preamp outputs are summed and pulse height analysis (8-channel) is performed to obtain energy data. A pulse shape discriminator (PSD) generates a veto signal if the event rise time exceeds a preset value indicating that the event originated from gamma rays or from charged particles. A veto signal from either the PSD or anticoincidence circuitry inhibits further processing of the event. Both types of veto pulses are scaled, accumulated, and periodically read out every 2.56 sec via the telemetry. In addition, there is circuitry to measure the time between events with an accuracy of less than 1.6% or 1μs, whichever is greater.

Table 6 summarizes MPC specifications. Appendix B, Table 3 gives total MPC counting rates (counts/sec, 1 - 10 keV) for sample source spectra, with unit normalization. The Crab would produce a counting rate of 10 x 220 = 2,200 counts/sec.

TABLE 6

(a)	Spatial resolution	1.5^{o} x 1.5^{o} FWFM
(b)	Temporal resolution	PHA: 2.56 seconds • Photon timing: $\leq$ 1.6% of measured intervals for intervals exceeding 64 μs; 1 μs for intervals less than 64 μs
(c)	Energy resolution	0.4 keV at 1.25 keV 1.2 keV at 5.9 keV
(d)	Sensitivity	1 count s^{-1} per 0.6 UFU (2-6 keV) or 1 count s^{-1} per 1.5 x 10^{-11} erg cm^{-2}-s^{-1} (0.1 - 6 keV Crab spectrum)
(e)	Active area	667 cm^{-2}
(f)	Background rejection	Anticoincidence on any two anodes and PSD, efficiency TBD

IV. OBSERVATORY OPERATION

A. Observing Program

The HEAO-B Observatory will be operated for one year starting in November 1978. Extended operation beyond one year may be possible. All use of the Observatory will be coordinated under the cognizance of the Director of the Observatory through the Mission Operations Office at Smithsonian Astrophysical Observatory. The operations of the Observatory will be directly controlled by the HEAO-B Operational Control Center (OCC) located at Goddard Space Flight Center. The full-time OCC staff will include MSFC and GSFC personnel, TRW subsystem engineers and ACDS monitors, and experiment representatives for instrument monitoring and observation scheduling functions.

The nature of the Observatory is such that any one of four separate instru ments may be placed at the focus of the telescope; in addition, auxiliary filters and gratings may be used. The choice of focal plane instrument, Observatory pointing direction, the use of filters or gratings, and the detailed configuration of each instrument is controlled from GSFC, either by real time ground command or by loading of the on-board stored command programmer (SCP). The complexity of the control function is such that all normal operations, including maneuvers, reconfigurations, and calibration sequences, will be carried out via the SCP. The 256-command SCP capacity, along with the capability for re-using certain command sequences will allow a nominal 12 to 18 hour loading cycle. The SCP loads will be prepared by the OCC staff several days in advance.

The Mission Operations Office at SAO will be responsible for collecting desired observations from the consortium members and from guest observers, and

integrating them into 6 month target lists. These inputs will be used to generate Master Observing Programs (MOP), SAO's controlling input to OCC during routine operations as shown in Figure 12.

The MOP entries will be of two types. The "general" or guideline entry will be an instruction to look at a given target (R.A. and Dec.) in a given instrument mode, for a given amount of time, during a certain time interval (typically several days). The "specific" entry will be similar, but may specify exact times (GMT) to start and/or stop the observation based on scientific constraints, e.g., coverage of some phase of a binary source or other time dependent phenomena. The MOP will be as realistic as possible in terms of available time, viewing constraints, reconfiguration optimization and momentum management, and will normally be sent to the OCC with at least a two-week lead time.

The MOP will be used by the OCC to generate a Detailed Observing Program (DOP). The DOP will schedule detailed start and stop time for a given observation, select guide stars, and specify all necessary instrument and spacecraft commands. DOP generation involves target sequencing to minimize gas consumption and reconfiguration times, and checking of restrictions due to sun angle, earth blocking, radiation background, moonlight, thermal power, maneuvering time, acquisition and/or settling time, and other constraints.

The DOP will be the prime data for the commands to be loaded in the SCP, as well as for scheduling any Real-Time Commands. In addition, the DOP will generate a permanent record of the planned observations. It should be noted that in general the exact target viewing times will not be known until the DOP is produced, approximately one or two weeks prior to the observation.

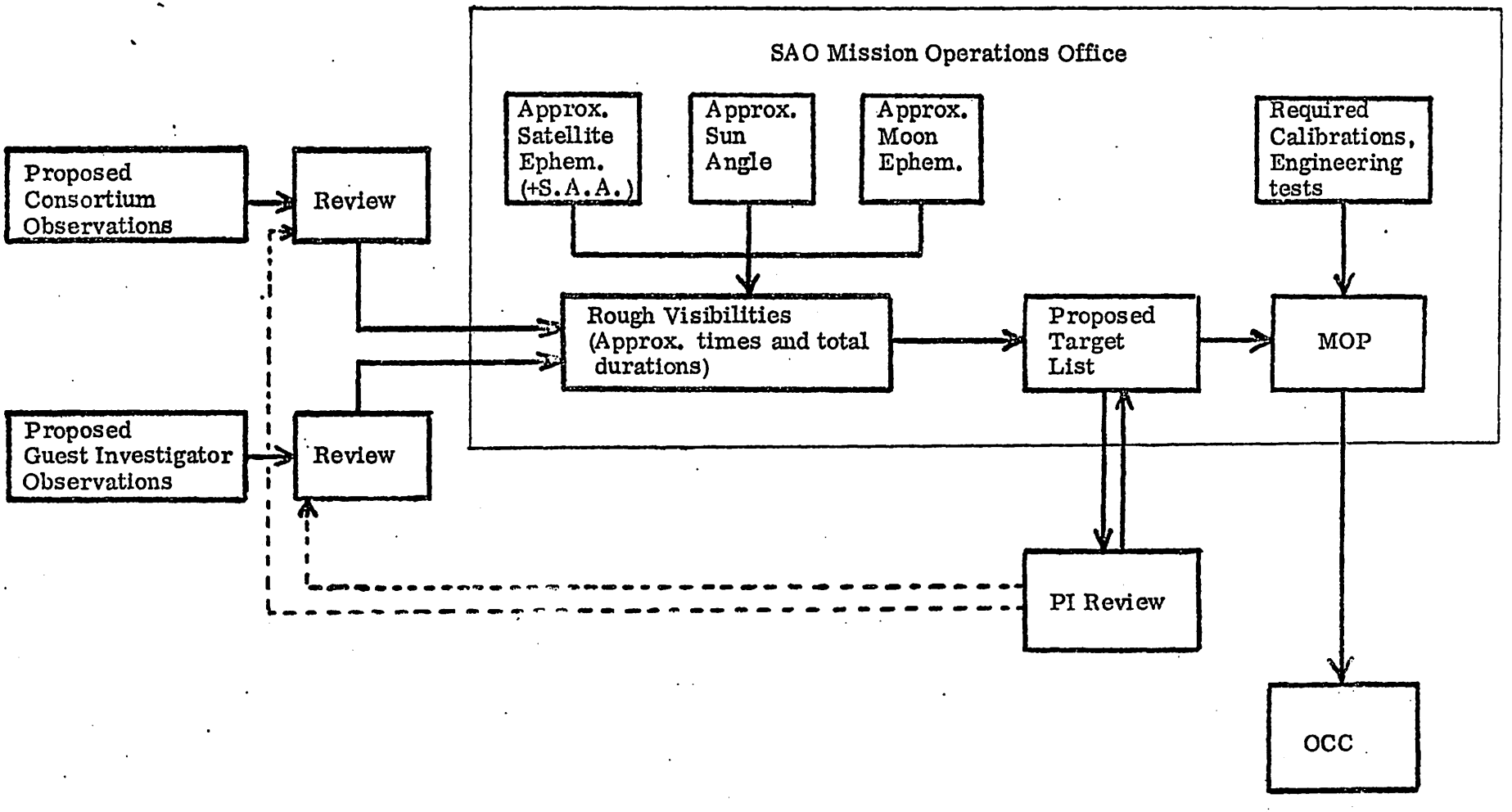

Figure 12 Observing Program Generation

B. Pointing and Visibility

The HEAO-B viewing axis (+X vehicle axis) may be directed within 1 arcmin of any selected point on the celestial sphere. The normal pointing directions must maintain the +Z vehicle axis within a 15^{o} half-cone angle centered about the solar vector. Thus, rough visibilities may be obtained by considering the $30^{o} \times 360^{o}$ band normal to the solar vector at any given date; this viewing swath covers the sky each six months. As a result, a typical source may only be observed twice a year for periods of duration of 1 month.

The Observatory has an active attitude control system, utilizing during normal operations gyros, reaction wheels, gas jets, three experiment star trackers, and an on-board computer. The gyros maintain an inertial reference; any torques (primarily gravity gradient) are compensated for by a change in the stored momentum of the reaction wheels. Reaction wheel momentum is automatically (or manually) unloaded as necessary by firing of gas jets. The gyro reference is continually updated when the star sensors are tracking the correct guide stars. Manual updates of the attitude reference and of gyro bias can be performed from the ground.

The target acquisition capability of the Observatory is limited by gas supply and power considerations and by the spacecraft's capability for stored commands. The ACDS memory is limited to 14 targets per load (nominally 12-18 hours).

Maneuvering times, attitude control capabilities, focal plane reconfiguration times, and operating requirements lead to the baseline that not more than two observations will normally be scheduled per orbit. This in turn implies a minimum useful observing interval of 1000 to 2000 seconds. Longer observations may be broken up into segments of this length.

The pointing of the +X axis is controlled and maintained as follows:

1. Accuracy of +X axis -- 1 arcminute half-cone angle (1σ).
2. Stability of +X axis -- 30 arcseconds in 1 hour (1σ).
3. Jitter of +X axis -- 1 arcsecond in 1 second (1σ).
4. Jitter about +X axis (roll) -- 20 arcseconds in 1 second (1σ).

Final attitude determination is performed at SAO. The star tracker data (along with gyro data as necessary) are compared with the known positions of the guide stars to obtain aspect to arcsecond precision. (The aspect solution and fiducial calibration data can then be used to superimpose image data.)

C. Conservation of Attitude Control Gas

The lifetime of HEAO-B is limited by the finite amount of gas carried. When this is gone, attitude control is lost. We expect that most of the gas will be used overcoming gravity gradient torques. These torques are minimum when pointing in or perpendicular to the plane of the orbit. Gravity gradient torque is maximum when pointed at an angle of 45° to the orbit plane.

Thus pointing direction affects mission life. Since the orbit plane precesses (period $\sim$ 53 days), one can minimize the torque by scheduling targets at an opportune time within the 30 day visibility window. However, this constrains target scheduling to an approximate 7 day window and interferes with observations of a target over an extended baseline, or with several instruments - in particular when results of one observation are necessary for scheduling a second. Assuming optimum scheduling, the relative dependence of gas usage on target declination has been calculated and is shown in Figure 13.

Targets at $|\delta| \sim 45^{\circ}$ use gas at a rate 5 times faster than targets at $|\delta| < 30^{\circ}$.

Clearly, optimization of a single observation is not important since the savings of gas in absolute terms is not large. If, however, the entire observing plan is optimized, the HEAO-B lifetime can be increased. The consortium observing program has already been revised to minimize gas usage; we encourage guest observers to keep these considerations in mind.

When planning observations, targets with $|\delta| < 30^{\circ}$ or $60^{\circ} < |\delta| < 75^{\circ}$ should be chosen if other considerations are equal. If selecting 10 objects to be observed from a list of 50, choose targets at low-gas-use declinations. If the program of the observation is to look at a specific astronomical object, there may be no choice but to operate at a rate of rapid gas usage.

D. Data Processing

The SAO facility will be based on Data General Eclipse minicomputers, with 800 and 1600 BPI tape drives, 90 megabyte disks, electrostatic printer/plotters, and graphics display facilities. Data will be reduced to either pictures, hard copy graphics, printout, or magnetic tape. Further analysis of data may be arranged with the Guest Observer Coordinator at SAO as appropriate. One computer will be dedicated largely to the Guest Observer program.

As a matter of routine, software will be available to do basic data processing. This will include producing HRI pictures (X-ray maps); IPC pictures in different energy bands; searching for sources in these fields, listing source locations, listing extended sources; obtaining pulse height spectra for IPC sources. OGS, SSS, and FPCS spectra will be available for visual inspection and the response of the instrument can be partially removed. Counting rate as a function of time will be obtained.

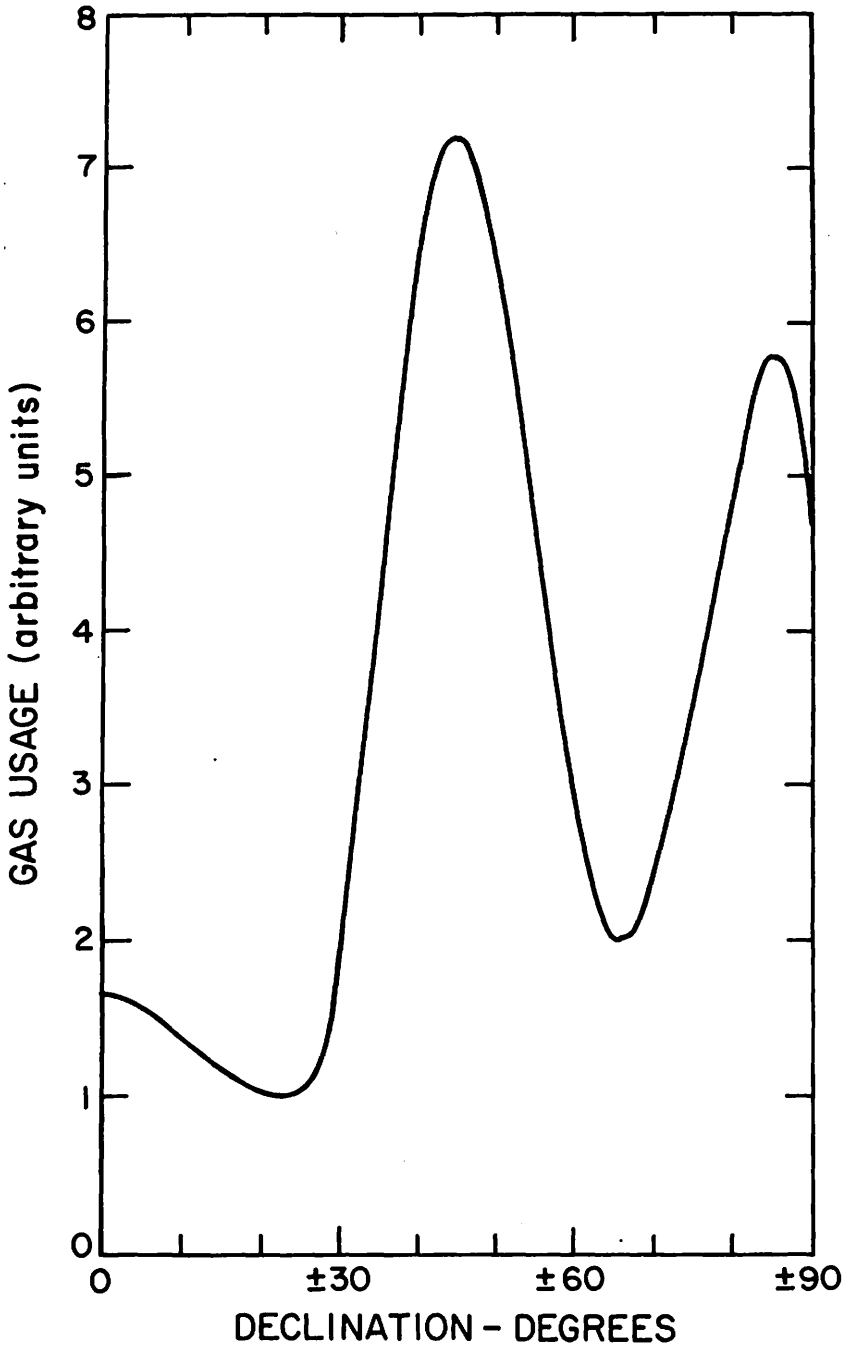

Figure 13. Relative amount of ACS gas used as a function of target declination.

It will be possible for Guest Observers to use a computer graphics display to inspect imaged X-ray fields and to select sources and background regions for additional processing.

We expect that Guest Observers will plan to spend ~ a week at SAO. Computer time and user assistance will be available. Data from an observation can be inspected and generally can be processed to the observer's specifications to the point where hard copy can then be sent back to the home institutions for more analysis or publication. Permanent records can be made as photographs, printout, or magnetic tape.

APPENDIX A

Observing Proposal Format

1. Title of Observation/Target Name:

   Category:

2. Observational Objectives:

3. Instrument:

4. Target Position(s) - R.A. (hr, min, sec); Dec. (deg, min, sec) [1950 coordinates]

5. Program (time required, sequence, etc.):

6. Overlapping Program (observations with other instruments, observations at other wavelengths, other HEAO-B observations):

7. Feasibility (will proposed observation fulfill objectives, signal and noise expected, total counts expected, etc.):

8. Scientific Objectives:

Observational Groups

I. Deep Surveys - Cosmology

[This category is devoted to the Consortium program of obtaining deep pictures of blank fields, for the purposes of studying the background and surveying the (extra-galactic) sky.]

II. Extragalactic Astronomy

- A. Clusters of Galaxies
- B. Active Galaxies and Abnormal Galaxies (Radio galaxies, Seyferts, etc.)
- C. Quasars
- D. Normal Galaxies

III. Galactic and Stellar Astronomy

- A. Neutron Stars, Black Holes and Binary X-ray Sources
- B. Globular Clusters & X-ray Bursters
- C. Miscellaneous Strong Galactic X-ray Sources
- D. Pulsars, Supernovae and Supernova Remnants
- E. Interstellar Medium
- F. Stellar Coronas, Flare Stars, White Dwarfs, Dwarf Novae
- G. Galactic Nucleus
- H. Novae and Nova-like Sources

IV. Other Aspects of the X-Ray Sky

- A. Surveys
- B. Locations
- C. Catalogs
- D. Time Variability
- E. Spectra
- F. Structure
- G. Miscellaneous Galactic Objects
- H. Solar System
- I. Other Targets

Sample Observing Proposal

1. Title of Observation/Target Name: Perseus Cluster

   Category: II A. 6

2. Observational Objectives:

   X-ray image of the central region of the Perseus cluster with 1.5' resolution, and study of time variability.

3. Instrument:

   IPC

4. Target Positions:

   $\alpha = 03^h\ 16^m\ 30^s, \quad \delta = 41^o\ 20'\ 00''$

5. Program:

   Total exposure of 3×10^4s divided in segments of $\sim 10^4$s each, separated by 2 weeks and 6 months.

6. Overlapping Program:

   III A.4.b (HRI), and CAL observations of entire cluster.

7. Feasibility:

   The UHURU counting rate is 47 cts s^{-1}. Spectrum is thermal with kT = 7 keV, $E_a = 0.5$ keV. Predicted IPC rate is $47/1.7 = 28$ cts s^{-1}. Assuming a uniform emission region of 30' diameter yields a surface brightness of 4×10^{-2} cts $(1')^{-2}\ s^{-1}$. A 3×10^4s exposure gives

   SOURCE = 2,700 cts $(1.'5)^{-2}$
   BKGD = 202 cts $(1.'5)^{-2}$

   So a feature of 2% contrast gives a 4σ effect. The limiting sensitivity for point sources in 10^4s is $2 \times 10^{-4}\ L_{Per} = 2.0 \times 10^{41}$ erg s^{-1} so normal galaxies will not be detected.

8. Scientific Objectives:

   To investigate the emission of the Perseus cluster. To try to discriminate between various models of the state of the intercluster gas, e.g. isothermal or adiabatic. Correlate the extended X-ray emission with radio and optical maps. To determine how much of the emission is in small diameter sources.

APPENDIX B

PREDICTED COUNTING RATES

FOR

NORMALIZED SOURCE SPECTRA

Table

Appendix B. 1a. HRI, 12 arc sec pixel, no filter

Exponential Spectrum: $\frac{dN}{dE} = (1.0)\ \frac{1}{E}\ e^{\frac{-E}{kT}}\ e^{-\left(\frac{E_a}{E}\right)^{8/3}}$

kT (keV)	$E_a = 0.0$	0.5	1.0	1.5	2.0	2.5	3.0
.500	1.010E+01	1.899E+00	3.750E-01	8.444E-02	2.340E-02	7.188E-03	2.377E-03
1.000	1.527E+01	4.349E+00	1.223E+00	4.023E-01	1.541E-01	6.361E-02	2.747E-02
1.500	1.805E+01	5.935E+00	1.910E+00	7.196E-01	3.090E-01	1.412E-01	6.682E-02
2.000	1.979E+01	7.003E+00	2.422E+00	9.776E-01	4.449E-01	2.140E-01	1.060E-01
2.500	2.097E+01	7.765E+00	2.807E+00	1.182E+00	5.570E-01	2.764E-01	1.407E-01
3.000	2.184E+01	8.333E+00	3.104E+00	1.344E+00	6.487E-01	3.286E-01	1.704E-01
4.000	2.301E+01	9.123E+00	3.531E+00	1.585E+00	7.875E-01	4.092E-01	2.172E-01
5.000	2.377E+01	9.645E+00	3.821E+00	1.752E+00	8.861E-01	4.676E-01	2.516E-01
6.000	2.430E+01	1.002E+01	4.031E+00	1.875E+00	9.594E-01	5.115E-01	2.777E-01
8.000	2.500E+01	1.051E+01	4.313E+00	2.042E+00	1.060E+00	5.727E-01	3.145E-01
10.000	2.544E+01	1.081E+01	4.493E+00	2.150E+00	1.127E+00	6.131E-01	3.390E-01
15.000	2.604E+01	1.125E+01	4.749E+00	2.305E+00	1.222E+00	6.719E-01	3.748E-01
20.000	2.635E+01	1.147E+01	4.883E+00	2.387E+00	1.273E+00	7.035E-01	3.943E-01

Power Law: $\frac{dN}{dE} = (1.0)\ E^{p}\ e^{-\left(\frac{E_a}{E}\right)^{8/3}}$

p	$E_a = 0.0$	0.5	1.0	1.5	2.0	2.5	3.0
-1.000	2.733E+01	1.218E+01	5.314E+00	2.655E+00	1.441E+00	8.084E-01	4.592E-01
-1.500	4.136E+01	1.226E+01	4.377E+00	1.907E+00	9.468E-01	4.973E-01	2.683E-01
-2.000	7.288E+01	1.308E+01	3.777E+00	1.414E+00	6.372E-01	3.117E-01	1.592E-01
-2.500	1.441E+02	1.465E+01	3.404E+00	1.081E+00	4.391E-01	1.990E-01	9.586E-02
-3.000	3.087E+02	1.710E+01	3.192E+00	8.515E-01	3.095E-01	1.294E-01	5.860E-02
-3.500	6.990E+02	2.065E+01	3.102E+00	6.892E-01	2.231E-01	8.568E-02	3.635E-02
-4.000	1.647E+03	2.570E+01	3.113E+00	5.723E-01	1.642E-01	5.770E-02	2.288E-02

Appendix B. 1b. HRI, 12 arc sec pixel, fliter: 2 mg/cm^2 Be + 5μ parylene N

Exponential Spectrum: $\frac{dN}{dE} = (1.0)\,\frac{1}{E}\,e^{\frac{-E}{kT}}\,e^{-\left(\frac{E_a}{E}\right)^{8/3}}$

kT (keV)	$E_a = 0.0$	0.5	1.0	1.5	2.0	2.5	3.0
.500	1.181E-01	1.061E-01	7.121E-02	3.387E-02	1.345E-02	5.023E-03	1.853E-03
1.000	5.281E-01	4.939E-01	3.602E-01	2.057E-01	1.028E-01	4.886E-02	2.283E-02
1.500	9.215E-01	8.686E-01	6.571E-01	4.006E-01	2.169E-01	1.120E-01	5.676E-02
2.000	1.236E+00	1.169E+00	9.014E-01	5.681E-01	3.203E-01	1.725E-01	9.105E-02
2.500	1.481E+00	1.405E+00	1.096E+00	7.047E-01	4.072E-01	2.248E-01	1.216E-01
3.000	1.676E+00	1.593E+00	1.251E+00	8.158E-01	4.791E-01	2.690E-01	1.479E-01
4.000	1.962E+00	1.868E+00	1.482E+00	9.825E-01	5.889E-01	3.377E-01	1.895E-01
5.000	2.160E+00	2.059E+00	1.643E+00	1.100E+00	6.677E-01	3.877E-01	2.202E-01
6.000	2.304E+00	2.199E+00	1.761E+00	1.188E+00	7.266E-01	4.254E-01	2.436E-01
8.000	2.501E+00	2.389E+00	1.923E+00	1.308E+00	8.083E-01	4.782E-01	2.765E-01
10.000	2.628E+00	2.512E+00	2.028E+00	1.386E+00	8.620E-01	5.131E-01	2.985E-01
15.000	2.809E+00	2.687E+00	2.178E+00	1.499E+00	9.397E-01	5.641E-01	3.308E-01
20.000	2.905E+00	2.780E+00	2.258E+00	1.559E+00	9.814E-01	5.915E-01	3.483E-01

Power Law: $\frac{dN}{dE} = (1.0)\,E^{p}\,e^{-\left(\frac{E_a}{E}\right)^{8/3}}$

p	$E_a = 0.0$	0.5	1.0	1.5	2.0	2.5	3.0
-1.000	3.217E+00	3.082E+00	2.517E+00	1.756E+00	1.119E+00	6.829E-01	4.069E-01
-1.500	2.365E+00	2.250E+00	1.780E+00	1.179E+00	7.109E-01	4.124E-01	2.352E-01
-2.000	1.797E+00	1.697E+00	1.296E+00	8.124E-01	4.612E-01	2.534E-01	1.379E-01
-2.500	1.409E+00	1.320E+00	9.715E-01	5.736E-01	3.054E-01	1.584E-01	8.198E-02
-3.000	1.138E+00	1.057E+00	7.481E-01	4.149E-01	2.064E-01	1.007E-01	4.945E-02
-3.500	9.449E-01	8.692E-01	5.909E-01	3.070E-01	1.423E-01	6.507E-02	3.025E-02
-4.000	8.047E-01	7.332E-01	4.780E-01	2.321E-01	9.992E-02	4.273E-02	1.876E-02

Appendix B. 1c. HRI, 12 arc sec pixel, filter: 1 mg/cm^2 Al + 5μ parylene N

Exponential Spectrum: $\frac{dN}{dE} = (1.0)\,\frac{1}{E}\,e^{\frac{-E}{kT}}\,e^{-\left(\frac{E_a}{E}\right)^{8/3}}$

kT (keV)	$E_a = 0.0$	0.5	1.0	1.5	2.0	2.5	3.0
.500	8.987E-02	8.034E-02	4.687E-02	1.705E-02	4.480E-03	1.195E-03	4.520E-04
1.000	3.244E-01	2.951E-01	1.873E-01	8.181E-02	3.075E-02	1.370E-02	7.457E-03
1.500	5.192E-01	4.759E-01	3.142E-01	1.505E-01	6.639E-02	3.468E-02	2.069E-02
2.000	6.662E-01	6.134E-01	4.147E-01	2.096E-01	1.006E-01	5.649E-02	3.508E-02
2.500	7.783E-01	7.188E-01	4.935E-01	2.583E-01	1.304E-01	7.627E-02	4.846E-02
3.000	8.659E-01	8.013E-01	5.563E-01	2.983E-01	1.558E-01	9.348E-02	6.026E-02
4.000	9.929E-01	9.215E-01	6.490E-01	3.591E-01	1.955E-01	1.210E-01	7.937E-02
5.000	1.080E+00	1.004E+00	7.137E-01	4.026E-01	2.246E-01	1.415E-01	9.379E-02
6.000	1.144E+00	1.065E+00	7.613E-01	4.351E-01	2.467E-01	1.572E-01	1.049E-01
8.000	1.230E+00	1.147E+00	8.264E-01	4.801E-01	2.778E-01	1.795E-01	1.207E-01
10.000	1.286E+00	1.200E+00	8.688E-01	5.098E-01	2.985E-01	1.945E-01	1.314E-01
15.000	1.365E+00	1.275E+00	9.295E-01	5.527E-01	3.287E-01	2.165E-01	1.472E-01
20.000	1.407E+00	1.315E+00	9.618E-01	5.757E-01	3.451E-01	2.285E-01	1.559E-01

Power Law: $\frac{dN}{dE} = (1.0)\,E^{p}\,e^{-\left(\frac{E_a}{E}\right)^{8/3}}$

p	$E_a = 0.0$	0.5	1.0	1.5	2.0	2.5	3.0
-1.000	1.542E+00	1.445E+00	1.067E+00	6.519E-01	3.999E-01	2.688E-01	1.851E-01
-1.500	1.221E+00	1.132E+00	7.944E-01	4.401E-01	2.422E-01	1.522E-01	1.013E-01
-2.000	1.008E+00	9.253E-01	6.186E-01	3.110E-01	1.516E-01	8.772E-02	5.612E-02
-2.500	8.608E-01	7.828E-01	5.003E-01	2.296E-01	9.840E-02	5.153E-02	3.146E-02
-3.000	7.552E-01	6.808E-01	4.175E-01	1.761E-01	6.628E-02	3.092E-02	1.785E-02
-3.500	6.773E-01	6.055E-01	3.571E-01	1.396E-01	4.636E-02	1.899E-02	1.026E-02
-4.000	6.186E-01	5.485E-01	3.117E-01	1.138E-01	3.360E-02	1.196E-02	5.980E-03

Appendix B. 1d. HRI, 500 line grating, 60 arc sec pixel, no filter, dispersed counts in first order

Exponential Spectrum: $\frac{dN}{dE} = (1.0)\ \frac{1}{E}\ e^{\frac{-E}{kT}}\ e^{-\left(\frac{E_a}{E}\right)^{8/3}}$

kT (keV)	$E_a = 0.0$	0.5	1.0	1.5	2.0	2.5	3.0
.500	1.371E+00	1.326E-01	2.063E-02	3.190E-03	6.438E-04	1.512E-04	4.076E-05
1.000	1.835E+00	2.800E-01	5.767E-02	1.263E-02	3.539E-03	1.148E-03	4.246E-04
1.500	2.052E+00	3.657E-01	8.371E-02	2.096E-02	6.606E-03	2.416E-03	9.984E-04
2.000	2.178E+00	4.198E-01	1.016E-01	2.725E-02	9.157E-03	3.564E-03	1.558E-03
2.500	2.260E+00	4.568E-01	1.145E-01	3.203E-02	1.120E-02	4.528E-03	2.047E-03
3.000	2.318E+00	4.837E-01	1.242E-01	3.575E-02	1.284E-02	5.326E-03	2.462E-03
4.000	2.394E+00	5.200E-01	1.377E-01	4.110E-02	1.527E-02	6.544E-03	3.111E-03
5.000	2.442E+00	5.434E-01	1.466E-01	4.475E-02	1.698E-02	7.417E-03	3.586E-03
6.000	2.475E+00	5.597E-01	1.529E-01	4.738E-02	1.823E-02	8.070E-03	3.946E-03
8.000	2.517E+00	5.810E-01	1.613E-01	5.094E-02	1.995E-02	8.975E-03	4.449E-03
10.000	2.543E+00	5.942E-01	1.666E-01	5.321E-02	2.107E-02	9.570E-03	4.784E-03
15.000	2.579E+00	6.124E-01	1.739E-01	5.643E-02	2.267E-02	1.043E-02	5.273E-03
20.000	2.597E+00	6.218E-01	1.778E-01	5.813E-02	2.351E-02	1.089E-02	5.537E-03

Power Law: $\frac{dN}{dE} = (1.0)\ E^{p}\ e^{-\left(\frac{E_a}{E}\right)^{8/3}}$

p	$E_a = 0.0$	0.5	1.0	1.5	2.0	2.5	3.0
-1.000	2.653E+00	6.510E-01	1.899E-01	6.358E-02	2.628E-02	1.242E-02	6.418E-03
-1.500	5.071E+00	7.233E-01	1.752E-01	4.976E-02	1.829E-02	7.899E-03	3.819E-03
-2.000	1.081E+01	8.322E-01	1.673E-01	4.012E-02	1.306E-02	5.131E-03	2.310E-03
-2.500	2.488E+01	9.868E-01	1.649E-01	3.323E-02	9.561E-03	3.404E-03	1.421E-03
-3.000	6.032E+01	1.202E+00	1.669E-01	2.822E-02	7.158E-03	2.303E-03	8.879E-04
-3.500	1.518E+02	1.501E+00	1.731E-01	2.450E-02	5.473E-03	1.589E-03	5.640E-04
-4.000	3.927E+02	1.920E+00	1.834E-01	2.171E-02	4.266E-03	1.117E-03	3.639E-04

Appendix B. 1e. HRI, 1,000 line grating, 60 arc sec pixel, no filter, dispersed counts in first order

Exponential Spectrum: $\frac{dN}{dE} = (1.0)\,\frac{1}{E}\,e^{\frac{-E}{kT}}\,e^{-\left(\frac{E_a}{E}\right)^{8/3}}$

kT (keV)	$E_a = 0.0$	0.5	1.0	1.5	2.0	2.5	3.0
.500	1.446E+00	2.807E-01	5.400E-02	1.047E-02	2.360E-03	5.771E-04	1.573E-04
1.000	2.188E+00	6.273E-01	1.623E-01	4.366E-02	1.325E-02	4.419E-03	1.647E-03
1.500	2.573E+00	8.399E-01	2.424E-01	7.336E-02	2.491E-02	9.331E-03	3.889E-03
2.000	2.808E+00	9.780E-01	2.988E-01	9.618E-02	3.466E-02	1.380E-02	6.084E-03
2.500	2.966E+00	1.074E+00	3.399E-01	1.136E-01	4.249E-02	1.755E-02	8.009E-03
3.000	3.079E+00	1.144E+00	3.710E-01	1.273E-01	4.879E-02	2.067E-02	9.647E-03
4.000	3.231E+00	1.241E+00	4.147E-01	1.469E-01	5.817E-02	2.544E-02	1.221E-02
5.000	3.328E+00	1.303E+00	4.438E-01	1.604E-01	6.475E-02	2.886E-02	1.410E-02
6.000	3.396E+00	1.347E+00	4.645E-01	1.702E-01	6.960E-02	3.142E-02	1.552E-02
8.000	3.483E+00	1.404E+00	4.921E-01	1.834E-01	7.623E-02	3.497E-02	1.752E-02
10.000	3.538E+00	1.440E+00	5.095E-01	1.918E-01	8.055E-02	3.732E-02	1.885E-02
15.000	3.612E+00	1.490E+00	5.340E-01	2.038E-01	8.674E-02	4.071E-02	2.080E-02
20.000	3.650E+00	1.516E+00	5.467E-01	2.101E-01	9.004E-02	4.253E-02	2.185E-02

Power Law: $\frac{dN}{dE} = (1.0)\,E^{p}\,e^{-\left(\frac{E_a}{E}\right)^{8/3}}$

p	$E_a = 0.0$	0.5	1.0	1.5	2.0	2.5	3.0
-1.000	3.769E+00	1.596E+00	5.872E-01	2.305E-01	1.008E-01	4.854E-02	2.536E-02
-1.500	5.811E+00	1.685E+00	5.200E-01	1.773E-01	6.968E-02	3.075E-02	1.503E-02
-2.000	1.020E+01	1.854E+00	4.771E-01	1.404E-01	4.944E-02	1.990E-02	9.056E-03
-2.500	1.983E+01	2.115E+00	4.520E-01	1.141E-01	3.593E-02	1.316E-02	5.551E-03
-3.000	4.149E+01	2.490E+00	4.410E-01	9.496E-02	2.670E-02	8.877E-03	3.460E-03
-3.500	9.136E+01	3.017E+00	4.418E-01	8.077E-02	2.026E-02	6.106E-03	2.192E-03
-4.000	2.087E+02	3.753E+00	4.535E-01	7.008E-02	1.566E-02	4.278E-03	1.412E-03

Appendix B. 2a. IPC A, no filter

Exponential Spectrum: $\frac{dN}{dE} = (1.0)\,\frac{1}{E}\,e^{\frac{-E}{kT}}\,e^{-\left(\frac{E_a}{E}\right)^{8/3}}$

kT (keV)	$E_a = 0.0$	0.5	1.0	1.5	2.0	2.5	3.0
.500	4.695E+01	1.062E+01	4.535E+00	1.774E+00	6.902E-01	2.656E-01	1.017E-01
1.000	8.468E+01	3.626E+01	2.068E+01	1.082E+01	5.460E+00	2.680E+00	1.289E+00
1.500	1.130E+02	5.901E+01	3.697E+01	2.124E+01	1.168E+01	6.215E+00	3.228E+00
2.000	1.339E+02	7.679E+01	5.036E+01	3.028E+01	1.737E+01	9.624E+00	5.194E+00
2.500	1.498E+02	9.059E+01	6.102E+01	3.770E+01	2.218E+01	1.258E+01	6.948E+00
3.000	1.622E+02	1.015E+02	6.956E+01	4.374E+01	2.617E+01	1.508E+01	8.457E+00
4.000	1.800E+02	1.174E+02	8.223E+01	5.285E+01	3.228E+01	1.898E+01	1.084E+01
5.000	1.922E+02	1.284E+02	9.108E+01	5.931E+01	3.668E+01	2.182E+01	1.261E+01
6.000	2.011E+02	1.364E+02	9.759E+01	6.410E+01	3.996E+01	2.396E+01	1.395E+01
8.000	2.131E+02	1.473E+02	1.065E+02	7.070E+01	4.452E+01	2.696E+01	1.584E+01
10.000	2.208E+02	1.543E+02	1.123E+02	7.501E+01	4.753E+01	2.894E+01	1.710E+01
15.000	2.317E+02	1.643E+02	1.205E+02	8.122E+01	5.188E+01	3.184E+01	1.895E+01
20.000	2.375E+02	1.696E+02	1.249E+02	8.454E+01	5.422E+01	3.340E+01	1.996E+01

Power Law: $\frac{dN}{dE} = (1.0)\,E^{p}\,e^{-\left(\frac{E_a}{E}\right)^{8/3}}$

p	$E_a = 0.0$	0.5	1.0	1.5	2.0	2.5	3.0
-1.000	2.561E+02	1.868E+02	1.393E+02	9.542E+01	6.193E+01	3.860E+01	2.332E+01
-1.500	2.744E+02	1.451E+02	9.942E+01	6.355E+01	3.902E+01	2.320E+01	1.345E+01
-2.000	3.789E+02	1.195E+02	7.375E+01	4.347E+01	2.508E+01	1.417E+01	7.868E+00
-2.500	6.488E+02	1.047E+02	5.690E+01	3.053E+01	1.645E+01	8.797E+00	4.663E+00
-3.000	1.273E+03	9.759E+01	4.567E+01	2.202E+01	1.101E+01	5.550E+00	2.801E+00
-3.500	2.693E+03	9.665E+01	3.812E+01	1.631E+01	7.519E+00	3.558E+00	1.705E+00
-4.000	5.942E+03	1.016E+02	3.305E+01	1.239E+01	5.234E+00	2.317E+00	1.052E+00

Appendix B. 2b. IPC A, filter: 2 mg/cm^2 Be + 5μ parylene N

Exponential Spectrum: $\frac{dN}{dE} = (1.0)\,\frac{1}{E}\,e^{\frac{-E}{kT}}\,e^{-\left(\frac{E_a}{E}\right)^{8/3}}$

kT (keV)	$E_a = 0.0$	0.5	1.0	1.5	2.0	2.5	3.0
.500	2.300E+00	2.164E+00	1.611E+00	9.288E-01	4.493E-01	1.969E-01	8.159E-02
1.000	1.323E+01	1.267E+01	1.025E+01	6.860E+00	4.005E+00	2.148E+00	1.093E+00
1.500	2.544E+01	2.450E+01	2.037E+01	1.433E+01	8.910E+00	5.115E+00	2.790E+00
2.000	3.589E+01	3.466E+01	2.922E+01	2.107E+01	1.351E+01	8.023E+00	4.530E+00
2.500	4.440E+01	4.295E+01	3.649E+01	2.671E+01	1.745E+01	1.057E+01	6.094E+00
3.000	5.130E+01	4.968E+01	4.244E+01	3.137E+01	2.074E+01	1.274E+01	7.444E+00
4.000	6.165E+01	5.979E+01	5.142E+01	3.846E+01	2.583E+01	1.613E+01	9.586E+00
5.000	6.896E+01	6.694E+01	5.779E+01	4.355E+01	2.951E+01	1.861E+01	1.118E+01
6.000	7.437E+01	7.222E+01	6.252E+01	4.734E+01	3.228E+01	2.049E+01	1.239E+01
8.000	8.181E+01	7.950E+01	6.904E+01	5.258E+01	3.613E+01	2.312E+01	1.410E+01
10.000	8.666E+01	8.425E+01	7.331E+01	5.604E+01	3.867E+01	2.487E+01	1.524E+01
15.000	9.363E+01	9.108E+01	7.946E+01	6.102E+01	4.237E+01	2.743E+01	1.692E+01
20.000	9.735E+01	9.472E+01	8.275E+01	6.370E+01	4.436E+01	2.881E+01	1.783E+01

Power Law: $\frac{dN}{dE} = (1.0)\,E^{p}\,e^{-\left(\frac{E_a}{E}\right)^{8/3}}$

p	$E_a = 0.0$	0.5	1.0	1.5	2.0	2.5	3.0
-1.000	1.095E+02	1.067E+02	9.354E+01	7.251E+01	5.095E+01	3.342E+01	2.089E+01
-1.500	7.409E+01	7.185E+01	6.181E+01	4.637E+01	3.136E+01	1.980E+01	1.194E+01
-2.000	5.154E+01	4.975E+01	4.188E+01	3.030E+01	1.966E+01	1.191E+01	6.916E+00
-2.500	3.687E+01	3.540E+01	2.910E+01	2.023E+01	1.255E+01	7.277E+00	4.057E+00
-3.000	2.711E+01	2.588E+01	2.072E+01	1.380E+01	8.150E+00	4.512E+00	2.410E+00
-3.500	2.049E+01	1.943E+01	1.512E+01	9.608E+00	5.388E+00	2.840E+00	1.450E+00
-4.000	1.589E+01	1.496E+01	1.130E+01	6.829E+00	3.624E+00	1.813E+00	8.839E-01

Appendix B. 2c. IPC A, filter: 1 mg/cm^2 Al + 5μ parylene N

Exponential Spectrum: $\frac{dN}{dE} = (1.0)\,\frac{1}{E}\,e^{\frac{-E}{kT}}\,e^{-\left(\frac{E_a}{E}\right)^{8/3}}$

kT (keV)	E_a = 0.0	0.5	1.0	1.5	2.0	2.5	3.0
.500	1.302E+00	1.193E+00	7.779E-01	3.434E-01	1.207E-01	4.599E-02	2.149E-02
1.000	5.767E+00	5.391E+00	3.894E+00	2.175E+00	1.129E+00	6.403E-01	3.827E-01
1.500	1.031E+01	9.732E+00	7.378E+00	4.561E+00	2.701E+00	1.696E+00	1.080E+00
2.000	1.416E+01	1.343E+01	1.046E+01	6.813E+00	4.288E+00	2.814E+00	1.843E+00
2.500	1.730E+01	1.647E+01	1.303E+01	8.759E+00	5.706E+00	3.836E+00	2.555E+00
3.000	1.987E+01	1.895E+01	1.516E+01	1.040E+01	6.928E+00	4.730E+00	3.183E+00
4.000	2.374E+01	2.271E+01	1.843E+01	1.297E+01	8.865E+00	6.163E+00	4.202E+00
5.000	2.651E+01	2.539E+01	2.078E+01	1.484E+01	1.030E+01	7.237E+00	4.971E+00
6.000	2.856E+01	2.739E+01	2.254E+01	1.625E+01	1.139E+01	8.059E+00	5.564E+00
8.000	3.140E+01	3.016E+01	2.499E+01	1.824E+01	1.294E+01	9.228E+00	6.410E+00
10.000	3.327E+01	3.199E+01	2.661E+01	1.956E+01	1.397E+01	1.001E+01	6.981E+00
15.000	3.597E+01	3.462E+01	2.895E+01	2.148E+01	1.549E+01	1.117E+01	7.825E+00
20.000	3.742E+01	3.603E+01	3.022E+01	2.252E+01	1.631E+01	1.180E+01	8.287E+00

Power Law: $\frac{dN}{dE} = (1.0)\,E^{p}\,e^{-\left(\frac{E_a}{E}\right)^{8/3}}$

p	E_a = 0.0	0.5	1.0	1.5	2.0	2.5	3.0
-1.000	4.219E+01	4.070E+01	3.440E+01	2.599E+01	1.907E+01	1.393E+01	9.848E+00
-1.500	2.914E+01	2.787E+01	2.264E+01	1.601E+01	1.106E+01	7.781E+00	5.371E+00
-2.000	2.115E+01	2.005E+01	1.559E+01	1.023E+01	6.558E+00	4.406E+00	2.959E+00
-2.500	1.609E+01	1.511E+01	1.124E+01	6.787E+00	3.985E+00	2.531E+00	1.647E+00
-3.000	1.276E+01	1.187E+01	8.451E+00	4.688E+00	2.489E+00	1.476E+00	9.271E-01
-3.500	1.048E+01	9.673E+00	6.603E+00	3.366E+00	1.602E+00	8.753E-01	5.274E-01
-4.000	8.866E+00	8.119E+00	5.330E+00	2.510E+00	1.064E+00	5.285E-01	3.034E-01

Appendix B. 2d. IPC B, no filter

Exponential Spectrum: $\frac{dN}{dE} = (1.0)\,\frac{1}{E}\,e^{\frac{-E}{kT}}\,e^{-\left(\frac{E_a}{E}\right)^{8/3}}$

kT (keV)	$E_a = 0.0$	0.5	1.0	1.5	2.0	2.5	3.0
.500	1.070E+01	4.551E+00	2.771E+00	1.339E+00	5.755E-01	2.342E-01	9.265E-02
1.000	2.951E+01	2.065E+01	1.482E+01	8.863E+00	4.782E+00	2.439E+00	1.201E+00
1.500	4.724E+01	3.693E+01	2.789E+01	1.787E+01	1.040E+01	5.718E+00	3.032E+00
2.000	6.153E+01	5.031E+01	3.894E+01	2.582E+01	1.559E+01	8.902E+00	4.897E+00
2.500	7.283E+01	6.097E+01	4.788E+01	3.240E+01	2.000E+01	1.168E+01	6.566E+00
3.000	8.183E+01	6.951E+01	5.511E+01	3.779E+01	2.366E+01	1.403E+01	8.004E+00
4.000	9.513E+01	8.218E+01	6.592E+01	4.596E+01	2.932E+01	1.770E+01	1.028E+01
5.000	1.044E+02	9.104E+01	7.353E+01	5.177E+01	3.339E+01	2.037E+01	1.197E+01
6.000	1.112E+02	9.755E+01	7.915E+01	5.609E+01	3.644E+01	2.240E+01	1.325E+01
8.000	1.205E+02	1.065E+02	8.687E+01	6.206E+01	4.068E+01	2.523E+01	1.506E+01
10.000	1.265E+02	1.122E+02	9.190E+01	6.597E+01	4.348E+01	2.711E+01	1.627E+01
15.000	1.351E+02	1.205E+02	9.912E+01	7.161E+01	4.753E+01	2.986E+01	1.804E+01
20.000	1.397E+02	1.249E+02	1.030E+02	7.462E+01	4.971E+01	3.134E+01	1.901E+01

Power Law: $\frac{dN}{dE} = (1.0)\,E^{p}\,e^{-\left(\frac{E_a}{E}\right)^{8/3}}$

p	$E_a = 0.0$	0.5	1.0	1.5	2.0	2.5	3.0
-1.000	1.546E+02	1.393E+02	1.155E+02	8.454E+01	5.692E+01	3.627E+01	2.223E+01
-1.500	1.233E+02	9.942E+01	7.933E+01	5.530E+01	3.550E+01	2.167E+01	1.278E+01
-2.000	1.160E+02	7.382E+01	5.618E+01	3.706E+01	2.258E+01	1.315E+01	7.442E+00
-2.500	1.372E+02	5.716E+01	4.105E+01	2.545E+01	1.464E+01	8.110E+00	4.392E+00
-3.000	2.040E+02	4.628E+01	3.095E+01	1.790E+01	9.675E+00	5.080E+00	2.626E+00
-3.500	3.566E+02	3.935E+01	2.407E+01	1.289E+01	6.516E+00	3.231E+00	1.591E+00
-4.000	6.817E+02	3.537E+01	1.930E+01	9.505E+00	4.471E+00	2.087E+00	9.765E-01

Appendix B. 2e. IPC B, filter: 2 mg/cm^2 Be + 5μ parylene N

Exponential Spectrum: $\frac{dN}{dE} = (1.0)\,\frac{1}{E}\,e^{\frac{-E}{kT}}\,e^{-\left(\frac{E_a}{E}\right)^{8/3}}$

kT (keV)	$E_a = 0.0$	0.5	1.0	1.5	2.0	2.5	3.0
.500	1.690E+00	1.605E+00	1.244E+00	7.593E-01	3.865E-01	1.758E-01	7.480E-02
1.000	1.063E+01	1.024E+01	8.511E+00	5.925E+00	3.583E+00	1.974E+00	1.024E+00
1.500	2.105E+01	2.038E+01	1.733E+01	1.261E+01	8.077E+00	4.744E+00	2.631E+00
2.000	3.013E+01	2.923E+01	2.516E+01	1.870E+01	1.233E+01	7.477E+00	4.287E+00
2.500	3.759E+01	3.653E+01	3.165E+01	2.383E+01	1.598E+01	9.879E+00	5.779E+00
3.000	4.368E+01	4.249E+01	3.698E+01	2.809E+01	1.905E+01	1.193E+01	7.069E+00
4.000	5.287E+01	5.148E+01	4.507E+01	3.460E+01	2.380E+01	1.513E+01	9.119E+00
5.000	5.939E+01	5.787E+01	5.083E+01	3.927E+01	2.724E+01	1.749E+01	1.064E+01
6.000	6.423E+01	6.262E+01	5.512E+01	4.276E+01	2.983E+01	1.927E+01	1.180E+01
8.000	7.090E+01	6.915E+01	6.105E+01	4.761E+01	3.344E+01	2.177E+01	1.344E+01
10.000	7.526E+01	7.343E+01	6.493E+01	5.080E+01	3.583E+01	2.344E+01	1.454E+01
15.000	8.154E+01	7.960E+01	7.054E+01	5.542E+01	3.930E+01	2.587E+01	1.615E+01
20.000	8.490E+01	8.289E+01	7.354E+01	5.790E+01	4.117E+01	2.719E+01	1.703E+01

Power Law: $\frac{dN}{dE} = (1.0)\,E^{p}\,e^{-\left(\frac{E_a}{E}\right)^{8/3}}$

p	$E_a = 0.0$	0.5	1.0	1.5	2.0	2.5	3.0
-1.000	9.591E+01	9.371E+01	8.341E+01	6.608E+01	4.738E+01	3.157E+01	1.997E+01
-1.500	6.355E+01	6.189E+01	5.424E+01	4.178E+01	2.895E+01	1.862E+01	1.138E+01
-2.000	4.319E+01	4.191E+01	3.610E+01	2.696E+01	1.800E+01	1.114E+01	6.566E+00
-2.500	3.010E+01	2.910E+01	2.459E+01	1.776E+01	1.138E+01	6.765E+00	3.836E+00
-3.000	2.152E+01	2.070E+01	1.713E+01	1.193E+01	7.325E+00	4.169E+00	2.270E+00
-3.500	1.576E+01	1.509E+01	1.221E+01	8.179E+00	4.795E+00	2.607E+00	1.360E+00
-4.000	1.182E+01	1.127E+01	8.900E+00	5.716E+00	3.191E+00	1.653E+00	8.251E-01

Appendix B. 2f. IPC B, filter: 1 mg/cm^2 Al + 5μ parylene N

Exponential Spectrum: $\frac{dN}{dE} = (1.0)\,\frac{1}{E}\,e^{\frac{-E}{kT}}\,e^{-\left(\frac{E_a}{E}\right)^{8/3}}$

kT (keV)	$E_a = 0.0$	0.5	1.0	1.5	2.0	2.5	3.0
.500	8.318E-01	7.714E-01	5.294E-01	2.538E-01	9.874E-02	4.124E-02	2.009E-02
1.000	4.101E+00	3.877E+00	2.944E+00	1.785E+00	1.007E+00	5.994E-01	3.648E-01
1.500	7.716E+00	7.358E+00	5.849E+00	3.896E+00	2.467E+00	1.604E+00	1.035E+00
2.000	1.089E+01	1.044E+01	8.500E+00	5.932E+00	3.958E+00	2.673E+00	1.771E+00
2.500	1.354E+01	1.301E+01	1.075E+01	7.711E+00	5.297E+00	3.654E+00	2.458E+00
3.000	1.573E+01	1.515E+01	1.264E+01	9.223E+00	6.454E+00	4.512E+00	3.066E+00
4.000	1.908E+01	1.842E+01	1.555E+01	1.159E+01	8.293E+00	5.891E+00	4.052E+00
5.000	2.149E+01	2.077E+01	1.766E+01	1.333E+01	9.659E+00	6.925E+00	4.797E+00
6.000	2.329E+01	2.253E+01	1.925E+01	1.465E+01	1.070E+01	7.718E+00	5.371E+00
8.000	2.580E+01	2.499E+01	2.147E+01	1.651E+01	1.217E+01	8.845E+00	6.192E+00
10.000	2.745E+01	2.661E+01	2.294E+01	1.774E+01	1.316E+01	9.602E+00	6.745E+00
15.000	2.985E+01	2.896E+01	2.509E+01	1.954E+01	1.461E+01	1.072E+01	7.565E+00
20.000	3.114E+01	3.023E+01	2.624E+01	2.052E+01	1.540E+01	1.133E+01	8.013E+00

Power Law: $\frac{dN}{dE} = (1.0)\,E^{p}\,e^{-\left(\frac{E_a}{E}\right)^{8/3}}$

p	$E_a = 0.0$	0.5	1.0	1.5	2.0	2.5	3.0
-1.000	3.542E+01	3.443E+01	3.008E+01	2.379E+01	1.804E+01	1.338E+01	9.528E+00
-1.500	2.343E+01	2.262E+01	1.914E+01	1.436E+01	1.037E+01	7.449E+00	5.185E+00
-2.000	1.624E+01	1.556E+01	1.270E+01	8.944E+00	6.080E+00	4.200E+00	2.850E+00
-2.500	1.178E+01	1.120E+01	8.790E+00	5.769E+00	3.643E+00	2.400E+00	1.583E+00
-3.000	8.914E+00	8.409E+00	6.348E+00	3.861E+00	2.237E+00	1.391E+00	8.882E-01
-3.500	7.007E+00	6.561E+00	4.769E+00	2.683E+00	1.411E+00	8.187E-01	5.038E-01
-4.000	5.688E+00	5.239E+00	3.710E+00	1.935E+00	9.164E-01	4.899E-01	2.888E-01

Appendix B. 3. Monitor Counter, 1 - 10 keV

Exponential Spectrum: $\frac{dN}{dE} = (1.0)\,\frac{1}{E}\,e^{\frac{-E}{kT}}\,e^{-\left(\frac{E_a}{E}\right)^{8/3}}$

kT (keV)	$E_a = 0.0$	0.5	1.0	1.5	2.0	2.5	3.0
.500	3.731E+00	3.585E+00	2.928E+00	1.949E+00	1.103E+00	5.702E-01	2.648E-01
1.000	3.109E+01	3.030E+01	2.662E+01	2.059E+01	1.445E+01	9.623E+00	6.271E+00
1.500	7.460E+01	7.312E+01	6.614E+01	5.424E+01	4.130E+01	3.020E+01	2.168E+01
2.000	1.228E+02	1.207E+02	1.109E+02	9.380E+01	7.453E+01	5.719E+01	4.315E+01
2.500	1.701E+02	1.676E+02	1.554E+02	1.340E+02	1.092E+02	8.629E+01	6.709E+01
3.000	2.144E+02	2.114E+02	1.974E+02	1.723E+02	1.429E+02	1.151E+02	9.130E+01
4.000	2.914E+02	2.879E+02	2.710E+02	2.403E+02	2.036E+02	1.680E+02	1.365E+02
5.000	3.542E+02	3.503E+02	3.313E+02	2.966E+02	2.545E+02	2.129E+02	1.756E+02
6.000	4.055E+02	4.012E+02	3.806E+02	3.429E+02	2.967E+02	2.505E+02	2.086E+02
8.000	4.830E+02	4.783E+02	4.555E+02	4.134E+02	3.614E+02	3.087E+02	2.600E+02
10.000	5.382E+02	5.332E+02	5.090E+02	4.641E+02	4.081E+02	3.509E+02	2.976E+02
15.000	6.244E+02	6.190E+02	5.926E+02	5.435E+02	4.818E+02	4.179E+02	3.575E+02
20.000	6.737E+02	6.681E+02	6.406E+02	5.892E+02	5.243E+02	4.567E+02	3.925E+02

Power Law: $\frac{dN}{dE} = (1.0)\,E^{p}\,e^{-\left(\frac{E_a}{E}\right)^{8/3}}$

p	$E_a = 0.0$	0.5	1.0	1.5	2.0	2.5	3.0
-1.000	8.528E+02	8.465E+02	8.151E+02	7.561E+02	6.805E+02	6.002E+02	5.224E+02
-1.500	4.227E+02	4.184E+02	3.977E+02	3.599E+02	3.141E+02	2.685E+02	2.269E+02
-2.000	2.230E+02	2.200E+02	2.057E+02	1.806E+02	1.518E+02	1.249E+02	1.019E+02
-2.500	1.254E+02	1.232E+02	1.130E+02	9.569E+01	7.689E+01	6.047E+01	4.732E+01
-3.000	7.489E+01	7.327E+01	6.575E+01	5.345E+01	4.080E+01	3.048E+01	2.276E+01
-3.500	4.730E+01	4.606E+01	4.038E+01	3.140E+01	2.265E+01	1.598E+01	1.133E+01
-4.000	3.138E+01	3.041E+01	2.603E+01	1.932E+01	1.312E+01	8.700E+00	5.830E+00

Appendix B. 4. UHURU Counter, "2-6 keV" (Side 1, 2.4 - 6.9 keV)

Exponential Spectrum: $\frac{dN}{dE} = (1.0)\,\frac{1}{E}\,e^{\frac{-E}{kT}}\,e^{-\left(\frac{E_a}{E}\right)^{8/3}}$

kT (keV)	$E_a = 0.0$	0.5	1.0	1.5	2.0	2.5	3.0
.500	4.020E-01	3.981E-01	3.776E-01	3.347E-01	2.723E-01	2.012E-01	1.348E-01
1.000	9.169E+00	9.099E+00	8.735E+00	7.961E+00	6.807E+00	5.435E+00	4.064E+00
1.500	2.959E+01	2.940E+01	2.838E+01	2.621E+01	2.293E+01	1.895E+01	1.484E+01
2.000	5.528E+01	5.495E+01	5.322E+01	4.951E+01	4.385E+01	3.690E+01	2.960E+01
2.500	8.165E+01	8.119E+01	7.879E+01	7.362E+01	6.572E+01	5.591E+01	4.551E+01
3.000	1.066E+02	1.060E+02	1.030E+02	9.658E+01	8.665E+01	7.428E+01	6.103E+01
4.000	1.500E+02	1.493E+02	1.453E+02	1.367E+02	1.234E+02	1.068E+02	8.877E+01
5.000	1.850E+02	1.841E+02	1.794E+02	1.692E+02	1.533E+02	1.334E+02	1.116E+02
6.000	2.132E+02	2.122E+02	2.069E+02	1.953E+02	1.775E+02	1.550E+02	1.303E+02
8.000	2.550E+02	2.539E+02	2.477E+02	2.344E+02	2.136E+02	1.873E+02	1.584E+02
10.000	2.843E+02	2.830E+02	2.763E+02	2.617E+02	2.390E+02	2.102E+02	1.783E+02
15.000	3.292E+02	3.277E+02	3.202E+02	3.037E+02	2.781E+02	2.453E+02	2.090E+02
20.000	3.544E+02	3.529E+02	3.448E+02	3.273E+02	3.001E+02	2.652E+02	2.264E+02

Power Law: $\frac{dN}{dE} = (1.0)\,E^{p}\,e^{-\left(\frac{E_a}{E}\right)^{8/3}}$

p	$E_a = 0.0$	0.5	1.0	1.5	2.0	2.5	3.0
-1.000	4.434E+02	4.415E+02	4.319E+02	4.109E+02	3.780E+02	3.357E+02	2.884E+02
-1.500	2.148E+02	2.138E+02	2.087E+02	1.974E+02	1.800E+02	1.579E+02	1.336E+02
-2.000	1.062E+02	1.057E+02	1.029E+02	9.675E+01	8.737E+01	7.560E+01	6.292E+01
-2.500	5.360E+01	5.330E+01	5.174E+01	4.837E+01	4.323E+01	3.688E+01	3.014E+01
-3.000	2.759E+01	2.742E+01	2.655E+01	2.467E+01	2.181E+01	1.833E+01	1.469E+01
-3.500	1.448E+01	1.439E+01	1.389E+01	1.282E+01	1.122E+01	9.279E+00	7.291E+00
-4.000	7.740E+00	7.685E+00	7.399E+00	6.789E+00	5.877E+00	4.784E+00	3.682E+00

APPENDIX C

HEAO-B FOCAL PLANE CRYSTAL SPECTROMETER SENSITIVITY TO A KNOWN LINE

"E" is energy in keV.

"λ" is wavelength in A.

"AEFF" is the effective area in cm^2 for line detection assuming nominal rocking operation.

"RES" is nominal in-focus resolution $E/\Delta E$.

Counts are per unit photon/(cm^2 s keV) for continuum and photon/(cm^2 s) for line.

Minimum line flux is in photon/(cm^2 s) for several values of continuum flux at confidence level 0.9997.

Table	Time	Crystal	Energy Range
1a	1,000 sec	PET	1.9 - 3.4
1b	1,000 sec	ADP	1.2 - 2.1
1c	1,000 sec	TAP	0.7 - 1.2
1d	1,000 sec	RAP	0.5 - 0.8
1e	1,000 sec	PBL	0.26 - 0.45
1f	1,000 sec	PBS	0.18 - 0.32
2a	10,000 sec	PET	1.9 - 3.4
2b	10,000 sec	ADP	1.2 - 2.1
2c	10,000 sec	TAP	0.7 - 1.2
2d	10,000 sec	RAP	0.5 - 0.8
2e	10,000 sec	PBL	0.26 - 0.45
2f	10,000 sec	PBS	0.18 - 0.32

Appendix C. 1a. 1,000 sec, PET Crystal, 1.900 to 3.353 keV

E	λ	AEFF	RES	Non X-ray Counts	Counts Per Unit Flux Cont	Line	Min Line Flux For Cont Flux as Shown 10.	1.0	0.1	0.01	0.001
1.900	6.53	0.69	361.	3.0	8.4	690.	0.101	0.026	0.014	0.013	0.013
1.950	6.36	0.66	326.	3.0	8.7	661.	0.111	0.029	0.015	0.014	0.014
2.000	6.20	0.63	296.	3.0	9.0	632.	0.119	0.030	0.016	0.014	0.014
2.050	6.05	0.60	271.	3.0	9.3	604.	0.126	0.031	0.017	0.015	0.015
2.100	5.90	0.29	249.	3.0	9.7	289.	0.197	0.052	0.031	0.028	0.028
2.150	5.77	0.28	230.	3.0	10.3	285.	0.207	0.056	0.032	0.028	0.028
2.200	5.64	0.28	214.	3.0	10.8	281.	0.221	0.057	0.032	0.029	0.029
2.250	5.51	0.28	199.	3.0	11.3	276.	0.232	0.058	0.033	0.029	0.029
2.300	5.39	0.27	186.	3.0	11.7	272.	0.243	0.062	0.033	0.029	0.029
2.350	5.28	0.27	175.	3.0	12.2	267.	0.255	0.064	0.034	0.030	0.030
2.400	5.17	0.26	164.	2.9	12.6	262.	0.267	0.065	0.034	0.031	0.031
2.450	5.06	0.26	155.	2.9	13.1	257.	0.280	0.066	0.035	0.031	0.031
2.500	4.96	0.25	146.	2.9	13.3	249.	0.293	0.072	0.036	0.032	0.032
2.550	4.86	0.24	139.	2.9	13.3	237.	0.309	0.076	0.038	0.034	0.034
2.600	4.77	0.22	131.	2.8	13.2	225.	0.454	0.098	0.049	0.040	0.040
2.650	4.68	0.21	125.	2.8	13.1	213.	0.473	0.103	0.052	0.042	0.042
2.700	4.59	0.20	119.	2.8	13.0	202.	0.499	0.109	0.054	0.044	0.044
2.750	4.51	0.19	113.	2.7	12.9	192.	0.521	0.115	0.052	0.047	0.047
2.800	4.43	0.18	108.	2.7	12.8	182.	0.544	0.121	0.055	0.049	0.049
2.850	4.35	0.17	103.	2.6	12.6	172.	0.569	0.128	0.058	0.052	0.052
2.900	4.28	0.16	99.	2.6	12.4	163.	0.589	0.129	0.061	0.055	0.055
2.950	4.20	0.15	95.	2.5	12.2	154.	0.616	0.136	0.065	0.058	0.058
3.000	4.13	0.15	91.	2.5	12.0	146.	0.637	0.144	0.069	0.062	0.055
3.050	4.07	0.14	87.	2.4	11.8	138.	0.667	0.152	0.072	0.065	0.058

Appendix C. 1b. 1,000 sec, ADP Crystal, 1.211 to 2.133 keV

E	λ	AEFF	RES	Non X-ray Counts	Counts Per Unit Flux Cont	Line	Min Line Flux For Cont Flux as Shown 10.	1.0	0.1	0.01	0.001
1.210	10.25	0.39	2352.	2.7	0.9	392.	0.033	0.018	0.018	0.018	0.018
1.235	10.04	0.41	1637.	2.7	1.2	410.	0.034	0.019	0.017	0.017	0.017
1.260	9.84	0.43	1267.	2.7	1.6	425.	0.045	0.021	0.019	0.016	0.016
1.285	9.65	0.43	1037.	2.7	1.8	429.	0.047	0.021	0.019	0.016	0.016
1.310	9.46	0.43	879.	2.8	2.1	433.	0.051	0.021	0.018	0.016	0.016
1.335	9.29	0.44	763.	2.8	2.3	436.	0.053	0.023	0.018	0.016	0.016
1.360	9.12	0.44	673.	2.8	2.6	439.	0.073	0.027	0.021	0.021	0.021
1.385	8.95	0.44	602.	2.8	2.8	441.	0.077	0.027	0.020	0.020	0.020
1.410	8.79	0.44	544.	2.8	3.1	444.	0.081	0.029	0.020	0.020	0.020
1.435	8.64	0.45	496.	2.8	3.3	446.	0.085	0.029	0.020	0.020	0.020
1.460	8.49	0.45	455.	2.9	3.6	448.	0.089	0.029	0.020	0.020	0.020
1.485	8.35	0.45	420.	2.9	3.8	450.	0.091	0.031	0.022	0.020	0.020
1.510	8.21	0.46	390.	2.9	4.1	456.	0.090	0.031	0.022	0.020	0.020
1.535	8.08	0.46	363.	2.9	4.4	463.	0.093	0.030	0.022	0.019	0.019
1.560	7.95	0.47	340.	2.9	4.7	469.	0.096	0.030	0.021	0.019	0.019
1.585	7.82	0.48	319.	2.9	5.0	476.	0.101	0.032	0.021	0.019	0.019
1.610	7.70	0.48	301.	2.9	5.3	482.	0.104	0.031	0.021	0.019	0.019
1.635	7.58	0.49	284.	3.0	5.7	488.	0.106	0.033	0.020	0.018	0.018
1.660	7.47	0.24	269.	3.0	6.0	242.	0.144	0.045	0.029	0.029	0.029
1.685	7.36	0.24	255.	3.0	6.3	245.	0.167	0.053	0.033	0.033	0.033
1.710	7.25	0.25	242.	3.0	6.7	248.	0.174	0.052	0.032	0.032	0.032
1.735	7.15	0.25	231.	3.0	7.0	248.	0.181	0.052	0.032	0.032	0.032
1.760	7.04	0.25	220.	3.0	7.3	250.	0.184	0.056	0.032	0.032	0.032
1.785	6.95	0.25	210.	3.0	7.6	248.	0.189	0.056	0.032	0.032	0.032
1.810	6.85	0.24	201.	3.0	7.7	243.	0.197	0.058	0.033	0.033	0.033
1.835	6.76	0.24	193.	3.0	7.8	238.	0.201	0.059	0.038	0.034	0.034
1.860	6.67	0.23	185.	3.0	8.0	233.	0.210	0.060	0.039	0.034	0.034
1.885	6.58	0.23	177.	3.0	8.1	228.	0.219	0.061	0.039	0.035	0.035
1.910	6.49	0.22	171.	3.0	8.2	224.	0.224	0.063	0.040	0.036	0.036
1.935	6.41	0.22	164.	3.0	8.3	219.	0.229	0.064	0.041	0.037	0.037
1.960	6.33	0.21	158.	3.0	8.4	214.	0.238	0.065	0.042	0.037	0.037
1.985	6.25	0.21	153.	3.0	8.4	209.	0.244	0.072	0.043	0.038	0.038
2.010	6.17	0.20	147.	3.0	8.5	205.	0.254	0.073	0.044	0.039	0.039
2.035	6.09	0.20	142.	3.0	8.6	200.	0.260	0.075	0.045	0.040	0.040
2.060	6.02	0.20	138.	3.0	8.7	196.	0.268	0.092	0.051	0.046	0.046
2.085	5.95	0.19	133.	3.0	8.8	194.	0.277	0.098	0.052	0.047	0.047
2.110	5.88	0.19	129.	3.0	9.0	192.	0.285	0.099	0.052	0.047	0.047

Appendix C. 1c. 1,000 sec, TAP Crystal, 0.693 to 1.216 keV

E	λ	AEFF	RES	Non X-ray Counts	Counts Per Unit Flux Cont	Line	Min Line Flux For Cont Flux as Shown 10.	1.0	0.1	0.01	0.001
0.690	17.97	0.50	140.	1.9	5.4	503.	0.099	0.028	0.016	0.016	0.016
0.710	17.46	0.53	130.	2.0	6.3	535.	0.103	0.028	0.017	0.015	0.015
0.730	16.98	0.56	121.	2.0	7.1	558.	0.109	0.029	0.016	0.014	0.014
0.750	16.53	0.58	113.	2.0	7.9	579.	0.114	0.029	0.016	0.014	0.014
0.770	16.10	0.60	106.	2.1	8.7	597.	0.121	0.030	0.015	0.013	0.013
0.790	15.69	0.28	100.	2.1	8.8	284.	0.187	0.049	0.028	0.025	0.025
0.810	15.31	0.26	94.	2.1	8.5	256.	0.199	0.055	0.031	0.027	0.027
0.830	14.94	0.23	89.	2.2	8.0	227.	0.216	0.062	0.035	0.031	0.031
0.850	14.59	0.20	84.	2.2	7.3	195.	0.235	0.067	0.041	0.036	0.036
0.870	14.25	0.19	80.	2.2	7.4	187.	0.246	0.070	0.043	0.037	0.037
0.890	13.93	0.19	76.	2.3	8.1	193.	0.253	0.072	0.041	0.036	0.036
0.910	13.62	0.20	73.	2.3	8.8	200.	0.265	0.070	0.040	0.035	0.035
0.930	13.33	0.21	69.	2.3	9.6	206.	0.271	0.073	0.039	0.034	0.034
0.950	13.05	0.21	66.	2.3	10.3	212.	0.279	0.071	0.038	0.033	0.033
0.970	12.78	0.22	64.	2.4	11.1	217.	0.290	0.074	0.037	0.032	0.032
0.990	12.52	0.22	61.	2.4	11.9	222.	0.298	0.072	0.036	0.032	0.032
1.010	12.28	0.23	58.	2.4	12.7	226.	0.310	0.075	0.035	0.031	0.031
1.030	12.04	0.23	56.	2.5	13.6	232.	0.319	0.078	0.039	0.030	0.030
1.050	11.81	0.24	54.	2.5	14.6	239.	0.327	0.075	0.038	0.029	0.029
1.070	11.59	0.24	52.	2.5	15.7	245.	0.339	0.078	0.037	0.029	0.029
1.090	11.37	0.25	50.	2.5	16.7	251.	0.347	0.076	0.036	0.028	0.028
1.110	11.17	0.26	48.	2.5	17.8	256.	0.359	0.078	0.035	0.027	0.027
1.130	10.97	0.26	47.	2.6	19.0	262.	0.523	0.103	0.042	0.034	0.034
1.150	10.78	0.27	45.	2.6	20.1	267.	0.539	0.105	0.041	0.034	0.034
1.170	10.60	0.27	44.	2.6	21.3	272.	0.555	0.107	0.040	0.033	0.033
1.190	10.42	0.28	42.	2.6	22.5	278.	0.569	0.108	0.043	0.032	0.032
1.210	10.25	0.29	41.	2.7	24.3	289.	0.582	0.107	0.042	0.031	0.031

Appendix C. 1d. 1,000 sec, RAP Crystal, 0.492 to 0.831 keV

E	λ	AEFF	RES	Non X-ray Counts	Counts Per Unit Flux Cont	Line	Min Line Flux For Cont Flux as Shown 10.	1.0	0.1	0.01	0.001
0.490	25.30	0.10	937.	1.5	0.2	95.	0.084	0.063	0.063	0.063	0.063
0.500	24.80	0.10	689.	1.5	0.3	104.	0.087	0.058	0.058	0.058	0.058
0.510	24.31	0.11	558.	1.5	0.3	112.	0.080	0.053	0.053	0.053	0.053
0.520	23.84	0.13	474.	1.6	0.4	129.	0.078	0.054	0.047	0.047	0.047
0.530	23.39	0.13	414.	1.6	0.5	134.	0.082	0.052	0.045	0.045	0.045
0.540	22.96	0.10	370.	1.6	0.4	99.	0.132	0.081	0.071	0.071	0.071
0.550	22.54	0.11	334.	1.6	0.5	107.	0.131	0.075	0.066	0.066	0.066
0.560	22.14	0.11	306.	1.7	0.6	114.	0.122	0.070	0.061	0.061	0.061
0.570	21.75	0.12	282.	1.7	0.7	122.	0.123	0.066	0.057	0.057	0.057
0.580	21.38	0.13	262.	1.7	0.8	130.	0.123	0.062	0.054	0.054	0.054
0.590	21.01	0.14	244.	1.7	0.9	137.	0.124	0.066	0.051	0.051	0.051
0.600	20.66	0.14	229.	1.7	1.0	144.	0.125	0.062	0.049	0.049	0.049
0.610	20.33	0.15	215.	1.8	1.1	151.	0.126	0.059	0.046	0.046	0.046
0.620	20.00	0.16	204.	1.8	1.2	158.	0.133	0.057	0.051	0.044	0.044
0.630	19.68	0.17	193.	1.8	1.4	166.	0.132	0.054	0.048	0.042	0.042
0.640	19.37	0.17	183.	1.8	1.5	174.	0.132	0.057	0.046	0.040	0.040
0.650	19.07	0.18	174.	1.8	1.6	182.	0.132	0.055	0.044	0.039	0.039
0.660	18.79	0.19	167.	1.9	1.8	189.	0.132	0.053	0.042	0.042	0.037
0.670	18.51	0.20	159.	1.9	1.9	196.	0.138	0.051	0.041	0.041	0.041
0.680	18.23	0.20	152.	1.9	2.1	203.	0.138	0.049	0.039	0.039	0.039
0.690	17.97	0.21	146.	1.9	2.3	209.	0.138	0.053	0.038	0.038	0.038
0.700	17.71	0.22	141.	1.9	2.4	217.	0.143	0.051	0.037	0.037	0.037
0.710	17.46	0.22	135.	2.0	2.6	223.	0.144	0.049	0.036	0.036	0.036
0.720	17.22	0.23	130.	2.0	2.8	228.	0.145	0.048	0.035	0.035	0.035
0.730	16.98	0.23	126.	2.0	2.9	233.	0.150	0.052	0.034	0.034	0.034
0.740	16.75	0.24	121.	2.0	3.1	237.	0.152	0.051	0.034	0.034	0.034
0.750	16.53	0.24	117.	2.0	3.3	241.	0.153	0.050	0.033	0.033	0.033
0.760	16.31	0.25	113.	2.0	3.5	245.	0.155	0.049	0.033	0.033	0.033
0.770	16.10	0.25	110.	2.1	3.6	249.	0.161	0.048	0.032	0.032	0.032
0.780	15.90	0.25	106.	2.1	3.7	247.	0.162	0.053	0.032	0.032	0.032
0.790	15.69	0.24	103.	2.1	3.7	237.	0.169	0.055	0.034	0.034	0.034
0.800	15.50	0.23	100.	2.1	3.6	225.	0.177	0.053	0.035	0.035	0.035
0.810	15.31	0.11	97.	2.1	3.5	107.	0.281	0.094	0.066	0.066	0.066
0.820	15.12	0.10	94.	2.1	3.4	101.	0.288	0.099	0.069	0.069	0.069

Appendix C. 1e. 1,000 sec, PBL Crystal, 0.263 to 0.453 keV

E	λ	AEFF	RES	Non X-ray Counts	Counts Per Unit Flux Cont	Line	Min Line Flux For Cont Flux as Shown 10.	1.0	0.1	0.01	0.001
C.26C	47.69	0.83	77.	0.9	6.8	825.	0.C71	C.C18	0.008	0.007	0.007
0.265	46.79	C.84	74.	C.9	7.4	844.	0.073	0.018	C.CC8	C.CC7	C.C07
C.270	45.92	0.8E	71.	C.9	7.9	861.	0.077	0.019	0.008	0.CC7	C.C07
C.275	45.09	C.88	68.	0.9	8.5	878.	C.C8C	C.C18	C.CC8	0.CC7	0.007
0.28C	44.28	C.89	65.	1.C	9.1	893.	0.C82	C.C19	C.CC8	C.CC7	C.C07
0.285	43.50	C.0C	63.	1.C	C.C	2.	2.746	2.746	2.746	2.746	2.746
C.29C	42.75	0.00	61.	1.0	0.0	3.	2.447	2.C98	2.098	2.098	2.098
0.295	42.03	C.CC	59.	1.0	0.0	4.	1.907	1.635	1.635	1.635	1.635
0.300	41.33	0.00	57.	1.C	0.1	5.	1.513	1.297	1.297	1.297	1.297
C.305	40.65	0.01	55.	1.0	0.1	6.	1.22C	1.046	1.046	1.046	1.046
C.31C	4C.CC	C.C1	53.	1.C	0.1	7.	1.141	C.856	C.856	C.856	C.856
0.315	39.36	0.C1	52.	1.1	C.1	8.	C.947	0.710	C.710	0.71C	C.71C
C.32C	38.75	C.C1	50.	1.1	C.1	1C.	C.795	C.596	C.596	0.596	0.596
0.325	38.15	C.C1	49.	1.1	0.2	12.	0.759	C.5C6	C.506	C.5C6	C.506
0.330	37.57	0.01	47.	1.1	C.2	14.	0.708	0.495	0.425	0.425	C.425
C.335	37.01	0.02	46.	1.1	0.3	17.	0.596	0.417	0.358	0.358	0.358
0.340	36.47	C.02	45.	1.1	0.3	20.	0.559	0.356	C.305	C.305	0.305
0.345	35.94	0.02	44.	1.1	0.4	23.	0.525	0.306	0.263	0.263	C.263
C.35C	35.42	0.03	42.	1.2	C.5	26.	C.498	0.268	C.230	0.230	0.23C
C.355	34.93	C.C3	41.	1.2	0.5	3C.	0.439	C.236	C.203	C.203	0.203
0.360	34.44	C.03	4C.	1.2	C.6	33.	0.420	0.210	0.18C	C.18C	C.18C
C.365	33.97	0.04	39.	1.2	C.7	37.	C.4C2	C.214	0.161	0.161	0.161
0.37C	33.51	C.C4	38.	1.2	0.8	42.	0.392	C.191	C.143	C.143	0.143
0.375	33.06	0.05	37.	1.2	1.0	47.	0.385	0.171	0.150	0.128	C.128
C.380	32.63	0.05	37.	1.2	1.1	52.	0.367	0.155	0.135	0.116	0.116
C.385	32.2C	C.C6	36.	1.2	1.3	57.	0.351	C.14C	C.123	0.105	0.105
0.39C	31.79	C.C6	35.	1.3	1.4	63.	0.351	0.144	C.112	C.C9E	C.C96
C.395	31.39	0.07	34.	1.3	1.6	69.	C.335	0.131	C.102	0.C87	C.C87
C.4CC	31.CC	C.C8	33.	1.3	1.8	75.	C.333	C.12C	C.C93	C.C93	C.080
0.405	30.61	C.C8	33.	1.3	2.0	82.	0.502	0.159	C.11C	0.11C	C.11C
0.410	30.24	0.09	32.	1.3	2.2	88.	C.498	0.158	0.102	0.102	0.102
0.415	29.88	0.10	31.	1.3	2.5	95.	0.493	C.147	C.C94	0.094	0.094
0.420	29.52	0.10	31.	1.3	2.8	103.	0.495	0.146	0.087	0.C87	C.C87
0.425	29.17	0.11	30.	1.3	3.C	111.	0.496	0.144	0.090	0.081	0.081
C.43C	28.83	0.12	30.	1.4	3.4	119.	C.497	C.135	C.C84	0.076	0.076
0.435	28.5C	C.13	29.	1.4	3.7	127.	0.497	C.134	C.C79	C.C71	C.C71
C.440	28.18	0.13	28.	1.4	4.C	135.	C.5C4	C.133	0.074	0.067	C.C67
C.445	27.86	C.14	28.	1.4	4.4	144.	0.5C1	C.125	C.C7C	0.063	0.063
0.450	27.55	0.15	27.	1.4	4.8	153.	0.510	0.124	C.C65	0.C59	C.C59

Appendix C. 1f. 1,000 sec, PBS Crystal, 0.184 to 0.317 keV

E	λ	AEFF	RES	Non X-ray Counts	Counts Per Unit Flux Cont	Line	Min Line Flux For Cont Flux as Shown 10.	1.0	0.1	0.01	0.001
C.2CC	61.99	0.93	82.	0.7	7.0	927.	0.C46	C.C13	0.006	0.006	0.006
0.205	60.48	C.97	77.	0.7	7.8	974.	0.048	0.012	C.CC6	C.CC6	C.C06
0.210	59.04	1.02	73.	C.8	8.7	1C18.	0.C70	0.016	0.007	0.CC6	C.CC6
C.215	57.67	1.06	70.	0.8	9.6	1C61.	C.C73	C.C16	C.CC7	0.C06	0.006
0.22C	56.36	1.11	67.	C.8	10.6	1105.	0.075	C.C16	C.CC6	C.CC5	C.CC5
0.225	55.10	1.15	64.	C.8	11.6	1147.	C.078	0.017	0.007	0.C05	C.CC5
C.23C	53.91	1.19	61.	0.8	12.6	1186.	C.C81	C.C17	0.007	0.005	0.005
0.235	52.76	1.22	58.	0.8	13.7	1222.	0.085	0.017	C.007	C.C05	0.005
0.240	51.66	1.26	56.	0.8	14.8	1256.	0.088	0.018	0.006	0.005	0.005
C.245	50.61	1.29	54.	0.9	16.0	1285.	C.C92	C.C18	0.006	0.005	0.005
C.25C	49.59	1.32	52.	C.9	17.1	1319.	0.C95	C.C18	C.CC7	C.CC5	C.C05
0.255	48.62	1.35	5C.	C.9	18.3	1347.	0.C98	0.019	C.007	C.CC4	C.CC4
C.26C	47.69	1.38	48.	0.9	19.6	1376.	C.1C1	C.C19	C.CC7	0.004	0.004
0.265	46.79	1.41	46.	C.9	20.9	1407.	0.105	C.C19	C.CC6	C.CC4	C.C04
0.270	45.92	1.44	45.	C.9	22.2	1435.	0.108	0.020	0.006	0.CC4	C.C04
0.275	45.09	1.46	43.	0.9	23.6	1463.	0.112	0.020	0.007	0.004	0.004
.0.280	44.28	1.49	42.	1.0	25.0	1488.	0.116	0.02C	C.CC7	C.004	0.004
0.285	43.50	0.00	4C.	1.C	C.1	4.	1.922	1.648	1.648	1.648	1.648
C.290	42.75	0.00	39.	1.C	C.1	5.	1.468	1.259	1.259	1.259	1.259
C.295	42.03	C.C1	38.	1.0	0.1	6.	1.3CE	C.981	C.981	C.981	0.981
0.300	41.33	0.01	37.	1.C	C.2	8.	1.037	0.778	C.778	0.778	C.778
C.3C5	4C.65	0.01	36.	1.C	C.2	1C.	C.941	C.627	0.627	0.627	0.627
0.31C	4C.0C	C.C1	35.	1.0	0.2	12.	0.856	C.514	C.514	C.514	0.514

Appendix C. 2a. 10,000 sec, PET Crystal, 1.900 to 3.353 keV

E	λ	AEFF	RES	Non X-ray Counts	Counts Per Unit Flux Cont	Counts Per Unit Flux Line	Min Line Flux For Cont Flux as Shown 10.	1.0	0.1	0.01	0.001
1.900	6.53	0.69	361.	30.3	84.0	6899.	0.076	0.013	0.006	0.005	0.005
1.950	6.36	0.66	326.	30.3	87.5	6606.	0.082	0.014	0.006	0.005	0.005
2.000	6.20	0.63	296.	30.3	90.5	6319.	0.088	0.015	0.006	0.005	0.005
2.050	6.05	0.60	271.	30.3	93.1	6041.	0.095	0.016	0.007	0.006	0.006
2.100	5.90	0.29	249.	30.3	97.4	2891.	0.143	0.024	0.011	0.009	0.009
2.150	5.77	0.28	230.	30.2	102.6	2849.	0.151	0.025	0.011	0.009	0.009
2.200	5.64	0.28	214.	30.1	107.7	2806.	0.160	0.026	0.011	0.009	0.009
2.250	5.51	0.28	199.	30.0	112.6	2761.	0.169	0.028	0.012	0.009	0.009
2.300	5.39	0.27	186.	29.8	117.3	2715.	0.179	0.029	0.012	0.010	0.010
2.350	5.28	0.27	175.	29.6	121.9	2668.	0.188	0.030	0.012	0.010	0.009
2.400	5.17	0.26	164.	29.4	126.4	2619.	0.198	0.031	0.012	0.010	0.010
2.450	5.06	0.26	155.	29.2	130.6	2570.	0.208	0.032	0.012	0.010	0.010
2.500	4.96	0.25	146.	28.9	133.1	2490.	0.218	0.034	0.013	0.010	0.010
2.550	4.86	0.24	139.	28.6	132.8	2366.	0.229	0.035	0.014	0.011	0.011
2.600	4.77	0.22	131.	28.3	132.3	2248.	0.349	0.053	0.018	0.015	0.014
2.650	4.68	0.21	125.	28.0	131.5	2134.	0.366	0.055	0.019	0.015	0.015
2.700	4.59	0.20	119.	27.6	130.4	2024.	0.383	0.057	0.020	0.016	0.016
2.750	4.51	0.19	113.	27.2	129.2	1919.	0.400	0.060	0.021	0.017	0.016
2.800	4.43	0.18	108.	26.8	127.8	1819.	0.418	0.063	0.023	0.018	0.017
2.850	4.35	0.17	103.	26.4	126.1	1723.	0.436	0.066	0.023	0.019	0.018
2.900	4.28	0.16	99.	25.9	124.3	1631.	0.454	0.068	0.025	0.019	0.018
2.950	4.20	0.15	95.	25.4	122.4	1543.	0.473	0.071	0.025	0.020	0.019
3.000	4.13	0.15	91.	24.9	120.3	1459.	0.493	0.074	0.027	0.021	0.021
3.050	4.07	0.14	87.	24.4	118.1	1380.	0.512	0.078	0.028	0.022	0.021

Appendix C. 2b. 10,000 sec, ADP Crystal, 1.211 to 2.133 keV

E	λ	AEFF	RES	Non X-ray Counts	Counts Per Unit Flux Cont	Line	Min Line Flux For Cont Flux as Shown 10.	1.0	0.1	0.01	0.001
1.210	10.25	0.39	2352.	26.6	9.1	3924.	0.013	0.006	0.005	0.005	0.005
1.235	10.04	0.41	1637.	26.8	12.5	4104.	0.015	0.006	0.005	0.005	0.005
1.260	9.84	0.43	1267.	27.1	15.6	4250.	0.022	0.008	0.006	0.006	0.006
1.285	9.65	0.43	1037.	27.3	18.2	4290.	0.024	0.008	0.006	0.006	0.006
1.310	9.46	0.43	879.	27.5	20.8	4325.	0.027	0.008	0.006	0.006	0.006
1.335	9.29	0.44	763.	27.7	23.3	4357.	0.029	0.008	0.006	0.006	0.006
1.360	9.12	0.44	673.	27.9	25.7	4387.	0.044	0.011	0.008	0.007	0.007
1.385	8.95	0.44	602.	28.1	28.2	4413.	0.047	0.011	0.008	0.007	0.007
1.410	8.79	0.44	544.	28.3	30.6	4438.	0.050	0.012	0.008	0.007	0.007
1.435	8.64	0.45	496.	28.5	33.1	4460.	0.053	0.012	0.008	0.007	0.007
1.460	8.49	0.45	455.	28.6	35.5	4481.	0.056	0.012	0.008	0.007	0.007
1.485	8.35	0.45	420.	28.8	38.0	4500.	0.059	0.013	0.008	0.007	0.007
1.510	8.21	0.46	390.	29.0	40.9	4564.	0.062	0.013	0.008	0.007	0.007
1.535	8.08	0.46	363.	29.1	43.9	4629.	0.064	0.013	0.008	0.007	0.007
1.560	7.95	0.47	340.	29.2	47.0	4694.	0.067	0.013	0.008	0.007	0.007
1.585	7.82	0.48	319.	29.4	50.2	4760.	0.070	0.014	0.008	0.007	0.007
1.610	7.70	0.48	301.	29.5	53.4	4823.	0.073	0.014	0.008	0.007	0.007
1.635	7.58	0.49	284.	29.6	56.7	4884.	0.076	0.014	0.008	0.007	0.007
1.660	7.47	0.24	269.	29.7	60.1	2423.	0.087	0.017	0.010	0.009	0.009
1.685	7.36	0.24	255.	29.8	63.5	2450.	0.116	0.022	0.012	0.011	0.011
1.710	7.25	0.25	242.	29.9	67.0	2476.	0.120	0.023	0.012	0.010	0.010
1.735	7.15	0.25	231.	30.0	70.0	2482.	0.124	0.023	0.012	0.010	0.010
1.760	7.04	0.25	220.	30.0	73.5	2503.	0.128	0.023	0.012	0.010	0.010
1.785	6.95	0.25	210.	30.1	75.8	2484.	0.133	0.024	0.012	0.010	0.010
1.810	6.85	0.24	201.	30.2	77.1	2433.	0.138	0.025	0.012	0.011	0.011
1.835	6.76	0.24	193.	30.2	78.4	2383.	0.143	0.026	0.013	0.011	0.011
1.860	6.67	0.23	185.	30.2	79.6	2333.	0.148	0.026	0.013	0.011	0.011
1.885	6.58	0.23	177.	30.3	80.7	2284.	0.153	0.027	0.013	0.011	0.011
1.910	6.49	0.22	171.	30.3	81.7	2235.	0.158	0.028	0.013	0.012	0.012
1.935	6.41	0.22	164.	30.3	82.7	2187.	0.163	0.029	0.014	0.012	0.012
1.960	6.33	0.21	158.	30.3	83.6	2140.	0.168	0.029	0.014	0.012	0.012
1.985	6.25	0.21	153.	30.3	84.5	2093.	0.174	0.031	0.014	0.012	0.012
2.010	6.17	0.20	147.	30.3	85.3	2047.	0.179	0.031	0.015	0.013	0.013
2.035	6.09	0.20	142.	30.3	86.0	2001.	0.184	0.032	0.015	0.013	0.013
2.060	6.02	0.20	138.	30.3	86.7	1956.	0.275	0.046	0.020	0.017	0.017
2.085	5.95	0.19	133.	30.3	88.3	1935.	0.283	0.047	0.021	0.018	0.018
2.110	5.88	0.19	129.	30.3	90.3	1922.	0.290	0.048	0.021	0.018	0.018

Appendix C. 2c. 10,000 sec, TAP Crystal, 0.693 to 1.216 keV

E	λ	AEFF	RES	Non X-ray Counts	Counts Per Unit Flux Cont	Counts Per Unit Flux Line	Min Line Flux For Cont Flux as Shown 10.	1.0	0.1	0.01	0.001
C.69C	17.97	0.50	140.	19.2	54.2	5027.	0.C7C	C.012	0.006	0.005	0.005
0.710	17.46	C.53	13C.	19.5	62.6	5348.	0.074	0.013	C.CC6	C.CC5	C.C05
C.730	16.98	0.5E	121.	19.9	7C.5	5583.	0.079	0.013	0.00E	0.CC5	C.CC5
C.75C	16.53	0.58	113.	20.3	78.7	579C.	C.C84	C.C13	C.CC6	0.004	0.004
0.77C	16.1C	C.6C	1C6.	20.6	87.0	5972.	0.C8S	C.C14	C.CCE	C.CC5	C.CC4
0.790	15.69	0.28	1CC.	21.C	E8.5	2841.	0.132	0.021	0.009	C.CC7	C.C07
C.81C	15.31	0.26	94.	21.3	85.1	2564.	0.141	C.C23	0.010	0.008	0.008
0.830	14.94	0.23	89.	21.6	80.0	2267.	0.152	0.026	C.011	C.C09	0.009
0.850	14.59	0.20	84.	21.9	73.1	1955.	0.162	0.028	0.013	0.011	0.011
C.87C	14.25	0.19	80.	22.2	73.9	1867.	C.171	C.029	0.013	0.012	0.011
C.89C	13.93	C.19	76.	22.6	80.9	1934.	0.179	C.C3C	C.C13	C.C11	C.011
C.910	13.62	0.2C	73.	22.9	E8.3	2001.	0.187	0.031	0.013	C.C11	C.C11
C.93C	13.33	0.21	69.	23.1	95.9	2064.	C.195	C.C31	C.C13	0.011	0.011
C.95C	13.05	0.21	66.	23.4	103.4	2118.	0.2C3	C.C33	C.C13	C.C11	C.C10
0.970	12.78	0.22	64.	23.7	111.1	2169.	0.212	0.033	0.013	0.C11	C.C1C
C.990	12.52	0.22	61.	24.0	119.0	2217.	0.221	0.034	0.013	0.010	0.010
1.010	12.28	0.23	58.	24.3	127.1	2261.	0.230	0.035	C.C13	0.C10	0.010
1.030	12.04	0.23	56.	24.5	136.4	2321.	0.238	0.036	0.013	0.C1C	C.C1C
1.C50	11.81	0.24	54.	24.8	146.5	2386.	0.247	0.037	0.013	0.010	0.010
1.C7C	11.59	C.24	52.	25.0	156.8	2448.	0.257	C.C38	C.C13	C.C1C	C.C09
1.090	11.37	0.25	5C.	25.3	167.5	2508.	0.266	C.C39	C.C13	C.C1C	C.CC9
1.11C	11.17	0.26	48.	25.5	178.4	2565.	C.276	C.C40	0.013	0.009	0.009
1.13C	1C.97	C.26	47.	25.7	189.5	2619.	0.417	C.C58	C.C16	C.012	0.011
1.150	10.78	0.27	45.	25.9	200.9	2671.	0.431	0.059	0.016	C.C12	C.012
1.170	10.60	0.27	44.	26.2	212.5	2721.	0.447	0.061	0.016	0.012	0.011
1.19C	1C.42	0.28	42.	26.4	225.1	2776.	0.461	C.C62	C.C16	C.C12	0.011
1.210	10.25	C.29	41.	26.6	242.6	2885.	0.476	0.063	C.C16	C.C11	C.C11

Appendix C. 2d. 10,000 sec, RAP Crystal, 0.492 to 0.831 keV

E	λ	AEFF	RES	Non X-ray Counts	Counts Per Unit Flux Cont	Counts Per Unit Flux Line	Min Line Flux For Cont Flux as Shown 10.	1.0	0.1	0.01	0.001
0.490	25.30	0.10	937.	15.0	1.8	954.	0.028	0.019	0.018	0.018	0.018
0.500	24.80	0.10	889.	15.2	2.5	1039.	0.030	0.018	0.016	0.016	0.016
0.510	24.31	0.11	558.	15.5	3.3	1124.	0.031	0.017	0.015	0.015	0.015
0.520	23.84	0.13	474.	15.7	4.4	1289.	0.032	0.016	0.014	0.013	0.013
0.530	23.39	0.13	414.	15.9	5.2	1337.	0.031	0.016	0.013	0.013	0.013
0.540	22.96	0.10	370.	16.1	4.3	987.	0.053	0.026	0.023	0.022	0.022
0.550	22.54	0.11	334.	16.3	5.1	1066.	0.053	0.025	0.022	0.022	0.022
0.560	22.14	0.11	306.	16.6	5.9	1144.	0.055	0.024	0.020	0.020	0.020
0.570	21.75	0.12	282.	16.8	6.8	1221.	0.057	0.024	0.019	0.019	0.019
0.580	21.38	0.13	262.	17.0	7.8	1296.	0.059	0.022	0.019	0.018	0.018
0.590	21.01	0.14	244.	17.2	8.8	1370.	0.060	0.022	0.018	0.017	0.017
0.600	20.66	0.14	229.	17.4	9.9	1442.	0.062	0.021	0.017	0.017	0.016
0.610	20.33	0.15	215.	17.6	11.0	1513.	0.063	0.021	0.017	0.016	0.016
0.620	20.00	0.16	204.	17.8	12.2	1582.	0.066	0.021	0.016	0.015	0.015
0.630	19.68	0.17	193.	18.0	13.5	1663.	0.068	0.021	0.015	0.014	0.014
0.640	19.37	0.17	183.	18.2	14.9	1741.	0.070	0.021	0.014	0.014	0.014
0.650	19.07	0.18	174.	18.4	16.4	1816.	0.072	0.020	0.014	0.013	0.013
0.660	18.79	0.19	167.	18.6	17.8	1889.	0.074	0.020	0.014	0.013	0.013
0.670	18.51	0.20	159.	18.8	19.4	1960.	0.076	0.020	0.013	0.013	0.013
0.680	18.23	0.20	152.	19.0	20.9	2028.	0.078	0.020	0.013	0.012	0.012
0.690	17.97	0.21	146.	19.2	22.6	2095.	0.080	0.020	0.013	0.012	0.012
0.700	17.71	0.22	141.	19.4	24.3	2167.	0.083	0.019	0.012	0.012	0.012
0.710	17.46	0.22	135.	19.5	26.1	2228.	0.085	0.019	0.012	0.011	0.011
0.720	17.22	0.23	130.	19.7	27.7	2279.	0.088	0.019	0.012	0.011	0.011
0.730	16.98	0.23	126.	19.9	29.4	2326.	0.090	0.019	0.012	0.011	0.011
0.740	16.75	0.24	121.	20.1	31.1	2371.	0.092	0.019	0.012	0.011	0.011
0.750	16.53	0.24	117.	20.3	32.8	2413.	0.095	0.020	0.012	0.011	0.011
0.760	16.31	0.25	113.	20.4	34.5	2452.	0.097	0.020	0.012	0.011	0.011
0.770	16.10	0.25	110.	20.6	36.3	2489.	0.100	0.020	0.012	0.010	0.010
0.780	15.90	0.25	106.	20.8	37.3	2475.	0.103	0.021	0.012	0.011	0.011
0.790	15.69	0.24	103.	21.0	36.9	2367.	0.107	0.022	0.012	0.011	0.011
0.800	15.50	0.23	100.	21.1	36.3	2255.	0.111	0.023	0.013	0.012	0.012
0.810	15.31	0.11	97.	21.3	35.5	1069.	0.161	0.036	0.022	0.020	0.020
0.820	15.12	0.10	94.	21.5	34.5	1008.	0.167	0.039	0.023	0.021	0.021

Appendix C. 2e. 10,000 sec, PBL Crystal, 0.263 to 0.453 keV

E	λ	AEFF	RES	Non X-ray Counts	Counts Per Unit Flux Cont	Line	Min Line Flux For Cont Flux as Shown 10.	1.0	0.1	0.01	0.001
C.26C	47.69	0.83	77.	9.0	68.4	8253.	0.C51	C.CC8	0.C03	0.002	0.002
0.265	46.79	C.84	74.	9.2	73.8	8439.	0.054	0.008	C.CC3	C.CC2	C.C02
0.270	45.92	0.86	71.	9.3	79.4	8613.	0.056	0.008	0.003	0.CC2	C.CC2
C.275	45.C9	0.88	68.	9.5	85.C	8776.	C.C59	C.CC9	C.C03	0.002	0.002
0.280	44.28	C.89	65.	9.6	90.8	8928.	0.061	C.CC9	C.C03	C.CC2	C.C02
0.285	43.50	0.00	63.	9.7	C.2	22.	0.870	0.778	0.778	0.778	C.778
C.29C	42.75	0.00	61.	9.9	0.3	29.	0.699	C.594	0.594	0.594	0.594
0.295	42.03	C.CC	59.	10.0	0.4	37.	0.572	0.463	C.463	0.463	0.463
0.300	41.33	0.00	57.	10.2	0.6	46.	0.476	0.389	0.367	0.367	0.367
C.305	40.65	0.01	55.	10.3	0.7	57.	C.418	0.314	0.296	0.296	0.296
C.31C	4C.CC	C.C1	53.	10.4	0.9	70.	0.357	C.257	C.243	C.243	0.243
0.315	39.36	0.C1	52.	10.6	1.2	85.	0.319	0.213	C.213	C.2C1	C.2C1
C.32C	38.75	C.01	50.	10.7	1.4	1C1.	C.298	C.189	C.179	0.179	0.179
0.325	38.15	C.C1	49.	10.9	1.8	119.	0.27C	C.16C	C.152	C.152	C.152
0.330	37.57	0.01	47.	11.C	2.2	141.	0.255	0.142	0.127	0.127	C.127
C.335	37.01	0.02	46.	11.1	2.7	168.	C.233	0.119	0.107	0.107	0.107
0.340	36.47	C.C2	45.	11.3	3.3	197.	0.208	0.107	C.C91	C.C91	0.091
0.345	35.94	0.02	44.	11.4	3.9	228.	0.201	0.096	0.083	0.C79	C.C79
C.350	35.42	0.03	42.	11.5	4.6	261.	C.195	C.C84	0.073	0.069	0.069
C.355	34.93	C.C3	41.	11.7	5.4	296.	0.189	C.C78	C.C64	C.C61	C.061
0.360	34.44	C.03	4C.	11.8	6.3	334.	0.186	C.072	C.C57	C.C57	C.C57
C.365	33.97	0.04	39.	11.9	7.3	373.	C.185	C.C67	0.051	0.051	0.051
C.37C	33.51	C.C4	38.	12.1	8.4	419.	C.181	C.C62	C.C48	C.045	0.045
0.375	33.06	0.05	37.	12.2	9.7	467.	0.182	0.058	0.043	0.041	C.C41
C.380	32.63	0.05	37.	12.3	11.1	517.	0.180	0.054	0.039	0.037	0.037
C.385	32.2C	C.C6	36.	12.4	12.6	570.	0.182	C.C53	C.C35	C.033	0.033
0.390	31.79	C.CC	35.	12.6	14.2	627.	0.182	0.049	C.C34	C.C3C	C.C30
C.395	31.39	0.07	34.	12.7	16.1	688.	C.182	C.C48	C.031	0.C28	C.C28
C.4CC	31.CC	C.C8	33.	12.8	18.0	751.	C.182	C.C45	C.C28	C.027	C.025
0.405	30.61	0.C8	33.	12.9	2C.2	816.	0.338	C.C7C	C.C40	C.C38	C.C37
C.41C	30.24	0.09	32.	13.1	22.4	883.	C.341	0.068	0.038	0.035	0.035
0.415	29.88	0.1C	31.	13.2	24.9	954.	0.346	C.C66	C.037	0.032	0.032
0.420	29.52	0.1C	31.	13.3	27.6	1030.	0.350	0.065	0.034	0.C3C	C.030
0.425	29.17	0.11	30.	13.4	3C.5	11C8.	0.355	0.064	0.032	0.029	0.028
C.43C	28.83	0.12	3C.	13.6	33.5	1187.	C.36C	C.C63	C.C3C	C.027	0.026
0.435	28.5C	C.13	29.	13.7	36.7	1268.	0.364	C.C62	C.C29	C.C25	C.C25
C.440	28.18	0.13	28.	13.8	4C.1	135C.	0.37C	C.062	0.028	0.C24	C.C24
0.445	27.86	0.14	28.	13.9	43.7	1436.	0.376	C.C61	C.C26	C.023	0.022
0.450	27.55	0.15	27.	14.1	47.6	1528.	0.382	C.C62	C.C26	C.C22	C.C21

Appendix C. 2f. 10,000 sec, PBS Crystal, 0.184 to 0.317 keV

E	λ	AEFF	RES	Non X-ray Counts	Counts Per Unit Flux Cont	Line	Min Line Flux For Cont Flux as Shown 10.	1.0	0.1	0.01	0.001
C.2CC	61.99	0.93	82.	7.2	69.6	9266.	C.C32	C.CC5	0.002	0.001	0.001
0.205	60.48	C.97	77.	7.4	78.0	9741.	0.034	0.005	C.CC2	C.CC1	C.C01
0.210	59.04	1.02	73.	7.5	86.7	10181.	0.C52	0.007	0.002	0.CC1	C.CC1
C.215	57.67	1.CC	70.	7.7	95.8	10CC6.	C.C54	C.CC8	C.CC2	C.002	0.001
0.22C	56.36	1.11	67.	7.8	105.7	11051.	0.057	C.CC8	C.CC2	C.CC1	C.CC1
0.225	55.10	1.15	64.	8.C	115.9	11467.	C.060	0.CC8	0.CC2	C.CC1	C.CC1
C.23C	53.91	1.19	61.	8.1	126.4	11857.	C.C63	C.CC9	0.CC2	0.001	0.001
0.235	52.76	1.22	58.	8.3	137.2	12223.	0.066	0.009	C.002	C.C01	0.001
0.240	51.66	1.26	56.	8.4	148.3	12565.	0.068	0.009	0.002	0.CC1	0.CC1
C.245	50.61	1.29	54.	8.6	159.6	12885.	C.C72	C.CC9	C.002	0.001	0.001
C.25C	49.59	1.32	52.	8.7	171.2	13186.	0.C75	C.C1C	C.CC2	C.CC1	C.C01
C.255	48.62	1.35	5C.	8.9	183.1	13468.	C.C78	0.01C	C.CC2	C.CC1	C.CC1
C.26C	47.69	1.38	48.	9.C	195.6	13755.	C.C81	C.C1C	C.CC2	C.001	0.001
0.265	46.79	1.41	46.	9.2	208.9	14065.	0.C84	C.C11	C.CC2	C.CC1	C.C01
0.270	45.92	1.44	45.	9.3	222.4	14355.	0.088	0.011	0.002	0.CC1	C.CC1
C.275	45.09	1.46	43.	9.5	236.2	14626.	0.C91	C.012	0.002	0.001	0.001
0.28C	44.28	1.49	42.	9.6	250.3	14880.	0.094	0.012	C.CC2	C.C01	0.001
0.285	43.50	0.00	4C.	9.7	6.6	36.	0.604	0.467	0.467	0.467	C.467
C.29C	42.75	0.00	3).	9.9	C.9	48.	C.5C3	C.378	0.357	0.357	0.357
C.295	42.C3	C.C1	38.	1C.C	1.2	61.	0.441	C.294	C.278	C.278	0.278
0.300	41.33	C.C1	37.	1C.2	1.5	77.	0.389	0.233	C.220	C.22C	C.220
C.3C5	4C.65	0.01	36.	10.3	1.9	96.	C.345	C.199	0.178	0.178	0.178
0.31C	4C.CC	C.C1	35.	1C.4	2.5	117.	0.317	C.171	C.154	C.146	0.146